The value of the whole or the sum of the parts: The role of ventromedial prefrontal cortex in multi-attribute object evaluation

Gabriel Pelletier[1,2], Nadav Aridan[3], *Lesley K Fellows[1,2] & *Tom Schonberg[3,4]

[1] Department of Neurology and Neurosurgery, McGill University, Montreal, Canada

[2] Montreal Neurological Institute, Montreal, Canada

[3] Department of Neurobiology, Faculty of Life Sciences, Tel Aviv University, Tel Aviv, Israel

[4] Sagol School of Neuroscience, Tel Aviv University, Tel Aviv, Israel

* These authors have contributed equally to the work.

Authors declare no competing interests

Funding

This work was supported by grants from the Israeli Science Foundation (1798/15 and 2004/15) granted to Tom Schonberg and from the Canadian Institutes of Health Research (MOP-11920) and the Natural Sciences and Engineering Council of Canada (RGPIN-2016-06066) to Lesley Fellows. Gabriel Pelletier was supported by the Zavalkoff Family Foundation as part of the Brain@McGill and Tel Aviv University collaboration, and by a "Sandwich" Scholarship from the Council for Higher Education in Israel.

Acknowledgement

The authors would like to thank Tom Salomon and Shiran Oren for helpful discussions on study design and data analysis, and Anastasia Saliy Grigoryan for help with participant recruitment. We would also like to thank the staff of The Alfredo Federico Strauss Center for Computational Neuroimaging of Tel Aviv University for help with data collection.

ABSTRACT

Everyday decision-making commonly involves assigning values to complex objects with multiple value-relevant attributes. Drawing on what is known about complex object recognition, we hypothesized two routes to multi-attribute evaluation: assessing the value of the whole object based on attribute configuration, or summing individual attribute-values. In two samples of healthy human participants undergoing eye-tracking and fMRI while evaluating novel pseudo-objects, we found evidence for distinct forms of multi-attribute evaluation. Fixations to, and transitions between attributes differed systematically when value was associated with individual attributes or attribute configurations. Further, ventromedial prefrontal cortex (vmPFC) and the perirhinal cortex were engaged during evaluation specifically when configural processing was required. These results converge with our recent findings that damage to vmPFC disrupts decisions when evaluation requires configural processing, and not in evaluating "the sum of the parts". This suggests that multi-attribute decisions may engage distinct evaluation mechanisms relying on partially dissociable neural substrates.

INTRODUCTION

Choosing which snack to buy from a vending machine requires assessing the value of options based on multiple attributes (e.g. color, taste, healthiness). Value can be related to individual attributes (Suzuki, Cross, and O'Doherty 2017): for example if someone likes chocolate, all snacks containing this ingredient will be valued above those that do not. Value can also emerge from the combination of attributes, such as for chocolate-peanut snacks, where the combination of sweet and salty ingredients within the same snack might yield a value greater than the sum of the individual attributes.

The object processing literature has shown that there are distinct neural substrates representing the individual elements that make up complex objects and the holistic, configural combinations of those elements (Bussey and Saksida 2002). When recognizing complex objects, attribute-level and whole object-level processing rely on dissociable brain regions along the hierarchically organized ventral visual stream (VVS). Posterior regions are involved in processing individual attributes whereas more anterior regions contribute to holistic (configural) object representations (Riesenhuber and Poggio 1999). Lesions to the perirhinal cortex (PRC), a medial temporal lobe structure situated at the anterior end of the VVS, impair object discrimination based on attribute configuration but spare discrimination based on individual attributes (Bartko et al. 2007; Bussey, Saksida, and Murray 2005; Murray, Bussey, and Saksida 2007). Several fMRI studies have shown that BOLD activity in the human PRC is more sensitive to multi-attribute configuration than to the component attributes of objects, whereas the lateral occipital cortex

demonstrates higher sensitivity to single attributes compared to anterior regions of the VVS (Devlin and Price 2007; Erez et al. 2016). This suggests that configural object recognition is supported by the PRC, and that individual attribute representations at earlier stages of object processing are sufficient for object recognition or discrimination under certain conditions.

Leading neuroeconomic models suggest that the vmPFC encodes subjective value across stimuli as a "common currency" (Levy and Glimcher 2012), which might support flexible decision-making (Delgado et al. 2016). While many of these studies have presented multi-attribute objects (e.g. foods, trinkets), they have only rarely considered how the values of multiple attributes are combined. A handful of functional MRI studies have examined the neural correlates of options explicitly composed of multiple attributes. These have found that signal within the vmPFC reflects the integrated value of the component attributes when each independently contributes to value, i.e. when value is associated with individual elements of the option (Basten et al. 2010; Hunt, Dolan, and Behrens 2014; Kahnt et al. 2011; Kurtz-David et al. 2019; Lim, O'Doherty, and Rangel 2013; Park et al. 2011; Philiastides, Biele, and Heekeren 2010; Suzuki et al. 2017). However, this work does not address whether there are distinctions in the neural processes underlying value construction based on component attributes and value emerging from the holistic configuration of attributes.

There is some recent evidence that this distinction between configural and elemental processing is important in evaluation, just as it is known to be important in complex object recognition. We recently found that lesions to the ventromedial prefrontal cortex (vmPFC) impaired decisions between objects when value was associated with the configural arrangement of attributes, but spared decisions when value was associated with individual attributes (Pelletier and Fellows 2019).

Eye-tracking studies found that eye movements also distinguish between configural and elemental processing. In a reinforcement learning paradigm, the amount of time spent fixating an outcome-predicting cue varied with the extent to which participants used cue-configurations or separate cues for learning (Duncan et al. 2018). It has also been found that when recognizing faces, people make more gaze transitions between attributes (e.g., eyes, nose) when configural processing is primed, and fixations are longer when elemental processing is primed (Bombari, Mast, and Lobmaier 2009). It is still an open question whether eye-movements on complex objects differ between configural and elemental evaluation.

Here, we relied on the framework provided by object processing research to better understand how the brain recognizes the value of multi-attribute objects. We employ a triangulation approach (Munafò and Smith 2018) to test this idea, using fMRI and eye-tracking to examine the neural and behavioural correlates of multi-attribute valuation. We hypothesized that estimating value in the configural condition would engage the vmPFC and high-level object recognition regions (i.e. PRC) to a greater extent than elemental valuation. We further hypothesized that fixations to, and fixation transitions between, value-predictive attributes would differ between configural and elemental value conditions. We report data from two independent samples of healthy participants: one behavioural and eye-tracking study, and another that also included fMRI. The fMRI sample was based on a third pilot study to determine the sample size. All hypotheses and analysis steps were pre-registered (osf.io/4d2yr).

METHODS

Data were collected from three independent samples using the same experimental paradigm. This paradigm involved first learning and then reporting the monetary value of novel, multi-attribute pseudo-objects under elemental or configural conditions. We collected an initial behavioural sample to characterize learning, decision-making and eye gaze patterns. We then undertook a pilot fMRI study to estimate the sample size needed to detect effects of interest. Informed by the pilot study that was used to determine the sample size, a third sample underwent fMRI and eye-tracking. Data from the behavioural sample informed the pre-registration of eye-tracking hypotheses to be replicated in the fMRI sample.

Participants

Participants were recruited from the Tel Aviv University community via online advertising and through the Strauss Imaging Center's participant database. Participants were healthy volunteers, with normal or corrected-to-normal vision, without any history of psychiatric, neurological, or metabolic diagnoses, and not currently taking psychoactive medication. The study was approved by the ethics committee at Tel Aviv University and the institutional review board of the Sheba Tel-Hashomer Medical Center.

Behavioural study

Forty-two participants were recruited to take part in the behavioural experiment. Nine participants were excluded due to poor task performance according to the exclusion criteria detailed below. The final behavioural sample included 33 participants (15 women, mean age 22 y, range 18-32). Eye tracking data were not collected in three participants due to poor calibration of the eye-tracker.

fMRI pilot study

Imaging data were collected in a pilot sample of 8 participants (four women, mean age 25 y, range 21-31) to calculate the sample size needed to detect a significantly stronger modulation of value in the Configural compared to the Elemental trials in the vmPFC at an alpha level of 0.05 with 95% power. Power calculations were carried out with the fmripower software (http://fmripower.org/)(Mumford and Nichols 2008), averaging beta weights for the contrast of interest across all voxels of a pre-defined brain region. Based on these calculations, we pre-registered that 42 participants would be required. This sample size was also sufficient to detect a significant effect for the parametric modulation of value in the Configural condition alone, in the vmPFC (38 participants needed for 95% power). The vmPFC region of interest and the model used to analyse the pilot data are described below. Imaging data used for power and sample-size calculations are available on OpenNeuro (https://openneuro.org/datasets/ds002079/versions/1.0.0), and the code used to create the power curves and the vmPFC ROI mask are available with the pre-registration document (osf.io/4d2yr). Pilot participants were not included in the final sample.

fMRI study

Fifty-five participants were recruited to take part in the full fMRI experiment. Nine participants were excluded due to poor task performance in the scanner, according to the pre-registered exclusion criterion (detailed below). Three participants were excluded because of MR artefacts, and one participant was excluded due to excessive motion inside the scanner based on fMRIprep outputs (Esteban et al. 2019). The final fMRI sample thus included 42 participants (21 women, mean age 27 y, range 18-39). Eye-tracking data could not be collected in 9 participants due to reflections caused by MR-compatible vision correction glasses.

Experimental paradigm

The experimental paradigm was adapted from a recently published study (Pelletier and Fellows 2019). Participants learned the monetary values of novel multi-attribute pseudo-objects (fribbles) in two conditions (configural and elemental), after which they were scanned while bidding monetary amounts for the objects. Fribbles were developed to study object recognition, and are designed to mimic real-world objects (Williams 1998). They are composed of a main body and four appendages which we refer to as attributes, each available in three variations. Two fribble sets were used, one for each condition (randomly assigned for each participant); each set had the same body but different appendages.

In the configural condition, value was associated with the unique configuration (conjunction) of two attributes. In the elemental condition, value was associated with each of two individual attributes, which then could be combined to obtain the value of the whole object. Four different object sets were used across participants and the object set-condition assignment was counterbalanced. Learning order was counterbalanced across participants (configural followed by elemental and vice versa) and the order of object presentation was randomized in all experiment phases. An example of the stimuli as well as the value associations are shown on **Figure 1**. All four sets used can be found in the Supplementary Material (**Fig. S1**).

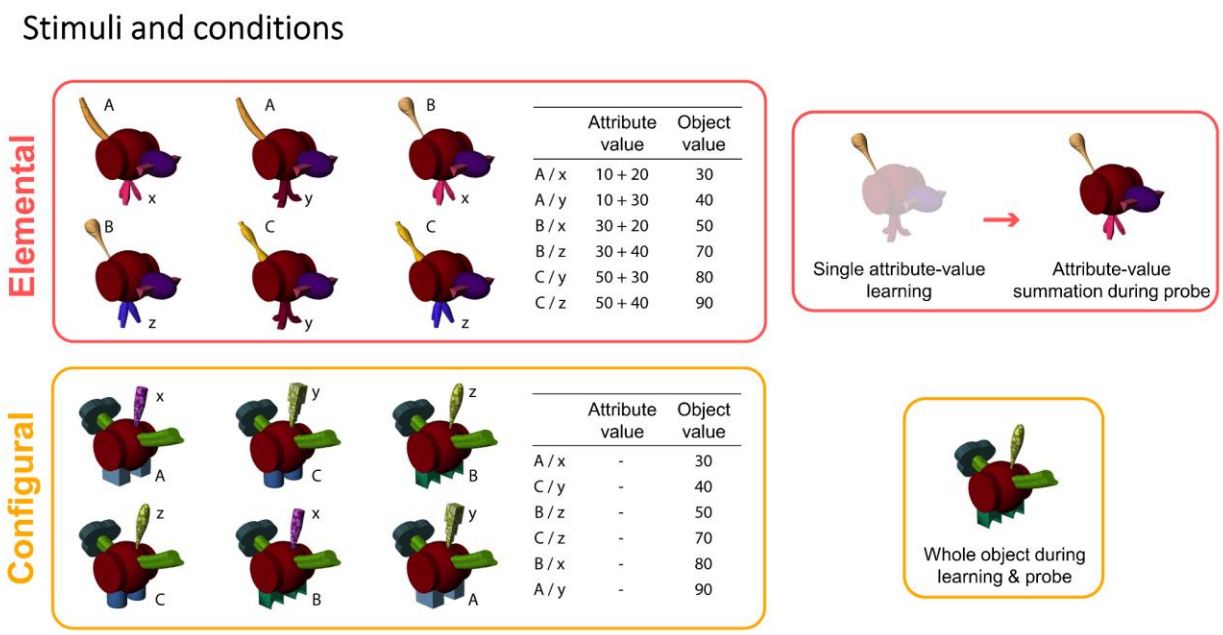

Figure 1. Stimuli and conditions. Example of fribbles sets and object-value associations. In the elemental condition, objects were masked during the learning blocks so it was clear that value was predicted by a single salient attribute. In the learning probe, the values of two attributes learned individually were then summed to generate the object-value.

Learning phase

Participants were instructed before the experiment that they were acting as business owners, buying and selling novel objects. Before acquiring objects in their own inventory, they began by observing objects being sold at auction to learn their market price.

The learning phase included five learning blocks and one learning probe per condition. A block began with a study slide displaying all 6 objects to be learned in that condition, along with the average value of

each object, giving the participant the opportunity to study the set for 60 s before the learning trials (**Fig. 2*A***). The learning trials began with the presentation of an object in the center of the screen above a rating scale, asking "How much is this item worth?". Participants had 5 s to provide a value estimate for the object, using the 'left' and 'right' arrow keys to move a continuous slider and the 'down' arrow key to confirm their response. Feedback was then provided indicating the actual selling price of the object, with a bright yellow bar and the corresponding numerical value overlaid on the same rating scale. The object, rating slider and feedback were displayed for 2 s, followed by 2 s fixation cross. Each learning block presented all 6 objects 6 times each in random order for a total of 36 trials. After five learning blocks, learning was assessed with a probe consisting of 24 trials of the 6 learned objects presented four times each, in random order. The structure of probe trials was identical to the learning trials, but no feedback was given after the value rating.

In the elemental condition, values were associated with individual attributes. During the learning blocks, the object's body and irrelevant attributes were occluded with a 50% transparent white mask, making the specific value-predictive attribute more salient (**Fig. 1**). Participants were explicitly told that value was associated only with the unmasked attribute. During the learning probe, objects were presented without masks, so all attributes were equally salient, and participants were instructed to sum the values of the two attributes they had learned.

In the configural condition, objects were displayed without masks during the entire learning phase, and the value of the object was associated with the unique configuration of two attributes. In this condition, participants could not learn object-values by associating value with any single attribute, because each attribute was included in both a relatively high-value and a relatively low-value object, as depicted in the object-value table (**Fig. 1**).

After learning, each of the 6 objects of the elemental condition had the same overall-value (sum of the two attribute-values) as one of the 6 configural objects. The object set in each condition contained 6 value-relevant attributes, each of which was part of two different objects in each set.

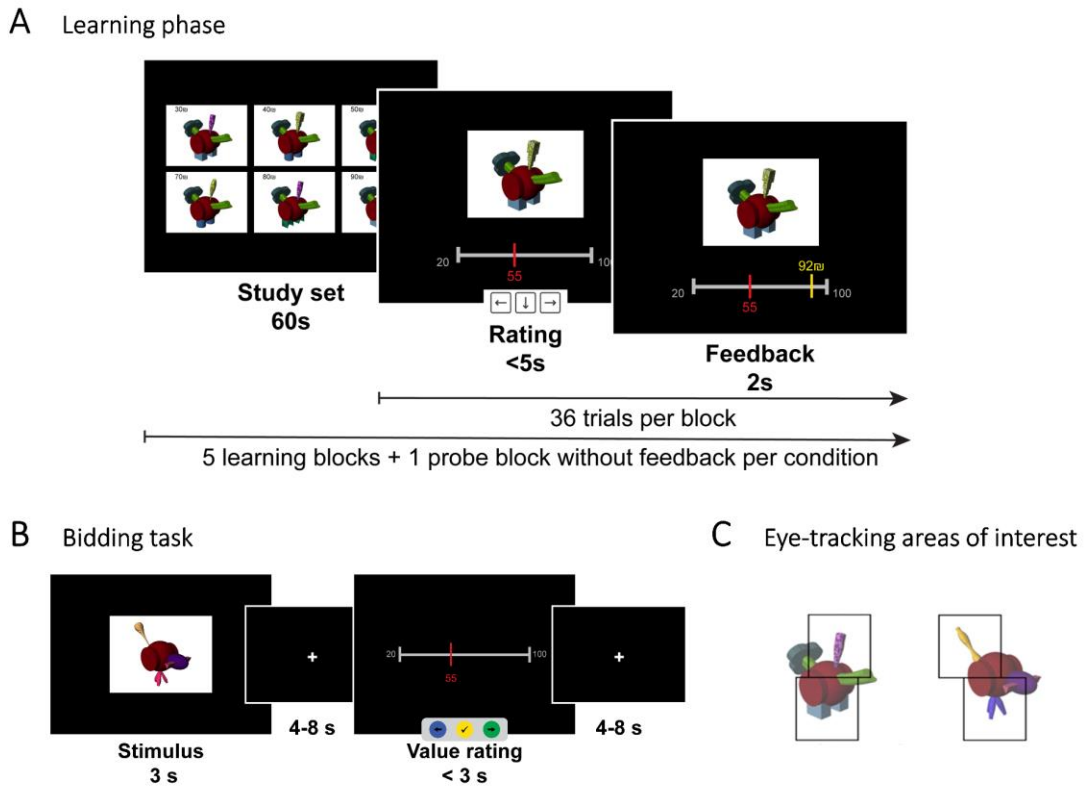

Figure 2. Experimental paradigm. A) Structure of a learning block. **B)** Trial structure of the bidding task (fMRI) task. **C)** Areas of interest (AOIs) used to assign eye fixations to the value-relevant attribute for eye-tracking analysis, depicted as black rectangles overlaid on an example object for each set.

Bidding task

After learning, participants placed monetary bids on the learned objects to acquire them for their inventory while eye movements were tracked and, in the fMRI studies, fMRI was acquired. The task comprised four runs (scans) each containing the 12 objects (6 per condition) repeated twice in random order for a total of 24 trials. The structure of a bidding trial is depicted in **Fig. 2*B***. Before the bidding task, participants performed one practice run to familiarize themselves with task timings.

To make the task incentive-compatible, participants were instructed beforehand that all auctions would be resolved at the end of the session. If they bid sufficiently close to, or higher, than the true (instructed) object's value, this object would be acquired and placed in their inventory. After the task, we would buy all the items in their inventory with a profit margin for the participant (similar to the situation where stores sell their products for a higher price than they paid from the manufacturer). The additional bonus compensation was calculated by summing the total amount paid by the experimenter

to buy the participant's inventory, minus the total of the bids placed by the participant to acquire these items. The margins were set so that the maximum bonus could not exceed 10 ILS (~$3 USD equivalent). Participants were told that they could not lose money in the experiment; if the total of their bids was substantially higher than the total retail value of their inventory, the bonus compensation was 0.

Anatomical scans and functional localizer task

After the bidding task, FLAIR and T1 anatomical scans and B0 field maps were acquired for the fMRI samples, with the parameters detailed bellow.

After structural scans, participants performed a functional localizer task adapted from (Watson, Wilding, and Graham 2012) to define participant-specific visual regions of interest for analysis of the bidding task. Images from four categories (faces, scenes, objects and scrambled objects) were presented in blocks of 15 s, each containing 20 images displayed for 300 ms with a 450 ms inter-stimulus interval. Participants were instructed to press a button using the index finger of the right hand when an image was repeated twice in a row (1-back). The task was comprised of 4 runs of 12 blocks each. A 15 s fixation block ended each run. One run contained three blocks of each image category in a counterbalanced order.

Data acquisition

Behavioural data

All phases of the experiment were programmed in Matlab (R2017b, The Mathworks, Inc.), using the Psychtoolbox extension (PTB-3) (Brainard 1997). During the learning phase, and during the bidding task for the behavioural sample, stimuli were displayed on a 21.5-inch monitor and responses were made using a standard keyboard. We recorded ratings and reaction time for each learning trial. During the bidding task in the fMRI, stimuli were presented on a NordicNeuroLab 32'' LCD display (1,920 x 1,080 pixels resolution, 120 Hz image refresh rate) that participants viewed through a mirror placed on the head coil. Participants responded using an MR-compatible response box. Value ratings, reaction time, and the entire path of the rating slider were recorded for each trial.

Eye tracking data

We recorded eye gaze data during the bidding task using the Eyelink 1000 Plus (SR research Ltd., Kanata, Ontario, Canada), sampled at 500 Hz. Nine-point calibration and validation were carried out before each run of the task.

fMRI data

Imaging data were acquired using a 3T Siemens Prisma MRI scanner and a 64-channel head coil. High-resolution T1-weighted structural images were acquired for anatomical localization using a magnetization prepared rapid gradient echo (MPRAGE) pulse sequence (Repetition time (TR) = 2.53 s, echo time (TE) = 2.99 ms, flip angle (FA) = 7°, field of view (FOV) = 224 × 224 × 176 mm, resolution = 1 × 1 × 1 mm).

Functional imaging data were acquired with a T2* weighted multiband echo planar imaging protocol (TR = 1,200 ms, TE = 30 ms, FA = 70 degrees, multiband acceleration factor of 4 and parallel imaging factor iPAT of 2, scanned in an interleaved fashion). Image resolution was 2 × 2 × 2 mm voxels (no gap between axial slices), FOV = 97 × 115 × 78 mm (112 × 112 × 76 acquisition matrix). All images were acquired at a 30° angle off the anterior–posterior commissures (AC–PC) line, to reduce signal dropout in the ventral frontal cortex (Deichmann et al. 2003). We also calculated field maps (b0) using the phase encoding polarity (PEPOLAR) technique, acquiring three images in two opposite phase encoding directions (anterior-posterior and posterior-anterior), to correct for susceptibility induced distortions.

Data and code sharing

Unthresholded whole-brain statistical maps are available at NeuroVault.org (https://neurovault.org/collections/MXWQPPCW/). Neuroimaging data necessary to recreate all analyses are available in brain imaging data structure format (BIDS) on OpenNeuro (https://openneuro.org/datasets/ds002994/versions/1.0.1). Behavioural and eye-tracking data, codes for behaviour, eye-tracking and fMRI analysis, and all experiment codes are available on GitHub (https://github.com/GabrielPelletier/fribblesFMRI_object-value-construction).

Data exclusion

Participants who performed poorly in the bidding fMRI task were excluded from analysis based on pre-registered exclusion criteria. Specifically, participants with average rating error ≥ 15 ILS in both conditions, or an average rating error ≥ 15 ILS for any single object were excluded. These criteria ensured that no participant using heuristics to estimate value (i.e. rough guessing based on a reduced number of attributes) was included in the final sample. Eye-tracking data were discarded for a trial if < 70% of samples could be labeled as fixations.

Statistical analysis

Behavioural data analysis

Value learning outside the scanner was assessed by the change in average rating error across learning blocks. Learning error was defined as the absolute difference between the rating provided by the subject and the true value of the object or attribute. A repeated-measure ANOVA with learning block (5 levels) and condition (2 levels) as within-subject factors was used to analyze rating error as learning unfolded. Group-level rating error in the learning probes was compared between conditions using a paired-sample t-test.

Accuracy in the bidding task inside the scanner was analyzed by calculating the average error (absolute difference between bid and instructed value) across the six repetitions for each of the 12 objects, as well as the average error by condition. Group-level bidding error was compared between conditions using a paired-sample t-test. Rating reaction times were similarly compared between conditions.

Eye-tracking data analysis

Eye-tracking data files in EyeLink (.edf) format were converted using the Edf2Mat Matlab Toolbox (https://github.com/uzh/edf-converter). Periods of eye blinks were removed from the data, after which the x and y coordinates and the duration of each fixation during the 3s of object presentation were extracted. We identified each fixation according to whether it fell on one or the other of the learned attributes, or neither. The attribute AOIs were defined by drawing the two largest equal-sized rectangles centered on the attributes of interest that did not overlap with each other. The same two AOIs were used for the 6 objects within each set. All AOIs covered an equal area of the visual field, although the positions varied between object sets. An example of the pre-registered AOIs is presented on **Fig. 2*C***. AOIs for all object sets along with their exact coordinates in screen pixels are shown in Supplementary material (**Fig. S1**).

For each subject and each condition, we calculated the average number of fixations per trial, and the number of fixations in each of the AOIs. We also calculated the average duration of individual fixations within each AOI and the total time spent fixating on each AOI. Finally, we calculated the average number of transitions from one attribute-AOI to the other. We counted as a transition every instance of a fixation falling on an AOI immediately preceded by a fixation falling on the other AOI. These variables were compared between conditions at the group-level using paired-sample t-tests.

fMRI data preprocessing

Raw imaging data in DICOM format were converted to NIfTI format and organized to fit the Brain Imaging Data Structure (BIDS) (Gorgolewski et al. 2016). Facial features were removed from the anatomical T1w images using pydeface (https://github.com/poldracklab/pydeface). Preprocessing was performed using fMRIPprep 1.3.0.post2 ((Esteban et al. 2019), RRID:SCR_016216), based on Nipype 1.1.8 ((Gorgolewski et al. 2011), RRID:SCR_002502).

Anatomical data preprocessing: The T1-weighted (T1w) image was corrected for intensity non-uniformity (INU) with N4BiasFieldCorrection (Tustison et al. 2010), distributed with ANTs 2.2.0 (Avants et al. 2008)(RRID:SCR_004757) and used as T1w-reference throughout the workflow. The T1w-reference was then skull-stripped using antsBrainExtraction.sh (ANTs 2.2.0), using OASIS30ANTs as target template. Brain surfaces were reconstructed using recon-all (FreeSurfer 6.0.1, RRID:SCR_001847, (Dale, Fischl, and Sereno 1999)), and the brain mask estimated previously was refined with a custom variation of the method to reconcile ANTs-derived and FreeSurfer-derived segmentations of the cortical gray-matter of Mindboggle (RRID:SCR_002438, (Klein et al. 2017)). Spatial normalization to the ICBM 152 Nonlinear Asymmetrical template version 2009c ((Fonov et al. 2009) RRID:SCR_008796) was performed through nonlinear registration with antsRegistration (ANTs 2.2.0), using brain-extracted versions of both T1w volume and template. Brain tissue segmentation of cerebrospinal fluid (CSF), white-matter (WM) and gray-matter (GM) was performed on the brain-extracted T1w using fast (FSL 5.0.9, RRID:SCR_002823, (Zhang, Brady, and Smith 2001)).

Functional data preprocessing: For each of the 8 BOLD runs per subject (across all tasks and sessions), the following preprocessing was performed. First, a reference volume and its skull-stripped version were generated using a custom methodology of fMRIPrep. A deformation field to correct for susceptibility distortions was estimated based on two echo-planar imaging (EPI) references with opposing phase-encoding directions, using 3dQwarp (Cox and Hyde 1997) (AFNI 20160207). Based on the estimated susceptibility distortion, an unwarped BOLD reference was calculated for a more accurate co-registration with the anatomical reference. The BOLD reference was then co-registered to the T1w reference using bbregister (FreeSurfer) which implements boundary-based registration (Greve and Fischl 2009). Co-registration was configured with nine degrees of freedom to account for distortions remaining in the BOLD reference. Head-motion parameters with respect to the BOLD reference (transformation matrices, and six corresponding rotation and translation parameters) were estimated before any spatiotemporal filtering using mcflirt (FSL 5.0.9, (Jenkinson et al. 2002)). The BOLD time-series (including slice-timing correction when applied) were resampled onto their original, native space by applying a

single composite transform to correct for head-motion and susceptibility distortions. These resampled BOLD time-series will be referred to as preprocessed BOLD in original space, or just preprocessed BOLD. The BOLD time-series were resampled to MNI152NLin2009cAsym standard space, generating a preprocessed BOLD run in MNI152NLin2009cAsym space. First, a reference volume and its skull-stripped version were generated using a custom methodology of fMRIPrep. Several confounding time-series were calculated based on the preprocessed BOLD: framewise displacement (FD), DVARS and three region-wise global signals. FD and DVARS were calculated for each functional run, both using their implementations in Nipype (following the definitions by (Power et al. 2014)). The three global signals were extracted within the CSF, the WM, and the whole-brain masks. Additionally, a set of physiological regressors were extracted to allow for component-based noise correction (CompCor, (Behzadi et al. 2007)). Principal components were estimated after high-pass filtering the preprocessed BOLD time-series (using a discrete cosine filter with 128s cut-off) for the two CompCor variants: temporal (tCompCor) and anatomical (aCompCor). Six tCompCor components are then calculated from the top 5% variable voxels within a mask covering the subcortical regions. This subcortical mask is obtained by heavily eroding the brain mask, which ensures it does not include cortical GM regions. For aCompCor, six components are calculated within the intersection of the aforementioned mask and the union of CSF and WM masks calculated in T1w space, after their projection to the native space of each functional run (using the inverse BOLD-to-T1w transformation). The head-motion estimates calculated in the correction step were also placed within the corresponding confounds file. All resamplings can be performed with a single interpolation step by composing all the pertinent transformations (i.e. head-motion transform matrices, susceptibility distortion correction when available, and co-registrations to anatomical and template spaces). Gridded (volumetric) resamplings were performed using antsApplyTransforms (ANTs), configured with Lanczos interpolation to minimize the smoothing effects of other kernels (Lanczos 1964). Non-gridded (surface) resamplings were performed using mri_vol2surf (FreeSurfer).

Confound files were created for each scan (each run of each task of each participant, in .tsv format), with the following columns: standard deviation of the root mean squared (RMS) intensity difference from one volume to the next (DVARS), six anatomical component based noise correction method (aCompCor), frame-wise displacement, and six motion parameters (translation and rotation each in 3 directions) as well as their squared and temporal derivatives (Friston 24-parameter model (Friston et al. 1996)). A single time point regressor (a single additional column) was added for each volume with FD

value larger than 0.9, in order to model out volumes with excessive motion. Scans with more than 15% scrubbed volumes were excluded from analysis.

fMRI data analysis

fMRI data were analyzed using FSL FEAT (fMRI Expert Analysis Tool) of FSL (Smith et al. 2004). A general linear model (GLM) was estimated to extract contrasts of parameter estimate at each voxel for each subject for each of the four fMRI runs (first level analysis). Contrasts of parameter estimate from the four runs were then averaged within participants using a fixed effect model (second level analysis). Group-level effects were estimated using a mixed effect model (FSL's FLAME-1).

General linear model: The GLM included one regressor modelling the 3-s object presentation time for Configural trials, and one regressor modelling object presentation for Elemental trials. The model also included one regressor modelling object presentation for the Configural trials modulated by the value rating of the object provided on each trial (mean centered), and the equivalent regressor for Elemental trials. We included four regressors modelling the rating epoch of the trial, with two unmodulated regressors modelling the rating scale for Configural trials and Elemental trials separately, and two regressors modelling the rating scale epoch modulated by value ratings (mean-centered) for Configural trials and Elemental trials separately. The duration of the rating event in these four regressors was set to the average rating reaction time across all participants and runs. Rating reaction times were accounted for in the model using a separate regressor modelling the rating epoch for all trials, modulated by the trial-wise reaction time (mean-centered). The duration was set to the maximum response time of 3 s in cases where the time limit was reached. To account for accuracy, two additional confound regressors were added to the model; one regressor modelling object presentation for all trials modulated by the absolute difference between the participant's rating and the instructed object value, and one regressor modelling the rating events with the same modulator. All regressors included in this GLM were convolved with a canonical double-gamma hemodynamic response function. Their temporal derivatives were also included in the model, with the motion and physiological confounds estimated by fMRIPrep as described above.

Regions of interest (ROI)

A vmPFC ROI was defined using the combination of the Harvard-Oxford regions frontal pole, frontal medial cortex, paracingulate gyrus and subcallosal cortex, falling between MNI x = -14 and 14 and $z < 0$, as in (Schonberg et al. 2014). This ROI was used for small volume correction where specified.

In addition, we defined four ROIs along the ventral visual stream of the brain; the perirhinal cortex (PRC), parahippocampal place area (PPA), fusiform face area (FFA) and the lateral occipital complex (LOC) using functional localizer data, as in (Erez et al. 2016). The PRC was defined based on a probabilistic map (Devlin and Price 2007) created by superimposing the PRC masks of 12 subjects, segmented based on anatomical guidelines in MNI-152 standard space. We thresholded the probabilistic map to keep voxels having more than 30% chance of belonging to the PRC, as in previous work (Erez et al. 2016). The lateral occipital complex (LOC) was defined as the region located along the lateral extent of the occipital pole that responded more strongly to objects than scrambled objects ($p < 0.001$, uncorrected). The fusiform face area (FFA) was defined as the region that responded more strongly to faces than objects. The PPA was defined as the region that responded more strongly to scenes than to objects. For each of these contrasts, a 10 mm radius sphere was drawn around the peak voxel in each hemisphere using FSL (fslmaths). To analyze brain activity in these regions during the bidding task, cope images from the second-level analysis (average of the four runs for each participant) were converted to percent signal change (as described in (Mumford 2007)), before averaging across all voxels within each ventral visual stream ROI. Group-level activations were compared against 0 using one-sample t-tests.

We also defined a hippocampus (HIP) ROI for exploratory analyses. HIP was defined using the Harvard-Oxford subcortical probabilistic atlas, defined as voxels having more than 30% chance of belonging to the hippocampus. ROI analyses including the HIP are reported in Supplementary Material (**Fig. S6**).

Functional connectivity analysis

Functional connectivity was assessed using generalized psychophysiological interaction analysis (gPPI), to reveal brain regions where BOLD time-series correlate significantly with the time-series of a target seed region in one condition more than another (McLaren et al., 2012). The seed region was defined based on the significant activation cluster found in the group-level analysis for the configural trials value-modulation contrast, small-volume corrected for the vmPFC ROI (**Fig. 6*A***). The seeds' neural response to configural and elemental trials were estimated by deconvolving the mean BOLD signal of all voxels inside the seed region (Gitelman et al. 2003).

The gPPI-GLM included the same regressors as the main GLM described above, plus two psychophysiological interaction (PPI) regressors of interest: one regressor modelling the seed region's response to configural trials, and one regressor modelling the seed region's response to elemental trials. These regressors were obtained by multiplying the seed region time-series with an indicator function for

object presentation of the corresponding condition, and then re-convolving the result with the double-gamma hemodynamic function. The model additionally included one regressor modelling the BOLD time-series of the seed region.

Inference criteria

For behavioural and eye-tracking analysis, we used the standard threshold of $p < 0.05$ for statistical significance, and we report exact *p*-values and effect sizes for all analyses. Neuroimaging data are reported at the group level with statistical maps thresholded at $Z > 3.1$ and cluster-based Gaussian Random Field corrected for multiple comparisons with a (whole brain corrected) cluster significance threshold of $p < 0.05$. We report analyses restricted to the vmPFC ROI using the same inference criteria, with increased sensitivity to detect effects in this region defined *a priori* due to fewer comparisons (small volume correction). Ventral visual stream ROI results are reported using the statistical threshold of $p < 0.05$, Bonferroni-corrected for four comparisons as the number of ROIs ($p < 0.0125$).

Deviations from preregistration

The most substantial deviation from the pre-registered analysis concerns the main GLM defined for fMRI analysis. The pre-registered model did not include accuracy confound regressors (one for value modulation during object presentation and one for value-modulation during value rating), which we added after behavioural data analysis revealed a trend difference in accuracy between conditions. We also controlled for reaction times differently than what was stated in the pre-registration, this was done due to a mistake in the pre-registered analysis plan that was different from the usual process of accounting for RT (Botvinik-Nezer, Salomon, and Schonberg 2020; Salomon et al. 2020; Schonberg et al. 2014). These changes to the GLM make the model more stringent and allow for a clearer interpretation of the value-related activations reported here, ruling out the possibility that they might reflect reaction-time or difficulty/accuracy.

RESULTS

Behaviour

We first present the behavioural results from the behavioural and fMRI studies, t0o establish the replicability of the behavioural effect.

Learning phase

Participants learned the value of novel multi-attribute objects under two conditions, elemental and configural. Learning behaviour differed between conditions in both the behavioural and the MRI sample (this phase of the task was performed outside the scanner in both studies), with configural associations being generally harder to learn than elemental ones, as detailed below.

Rating error decreased across learning trials and was generally higher in the configural condition as depicted in **Figure 3*A***. This was formalized by a repeated measures ANOVA with block and condition as within-subject factors, which revealed a main effect of block (behavioural sample $F_{4, 288} = 58.21$, $p < 0.001$, $\eta^2_p = 0.45$; fMRI sample $F_{4, 369} = 60.73$, $p < 0.001$, $\eta^2_p = 0.40$) and a main effect of condition (behavioural sample $F_{4, 288} = 372.14$, $p < 0.001$, $\eta^2_p = 0.56$; fMRI sample $F_{1, 369} = 470.84$, $p < 0.001$, $\eta^2_p = 0.56$) on rating error. We also found a significant block by condition interaction (behavioural sample $F_{4, 288} = 37.98$, $p < 0.001$, $\eta^2_p = 0.35$; fMRI sample $F_{4, 369} = 30.20$, $p < 0.001$, $\eta^2_p = 0.25$). This interaction reflects that accuracy becomes more similar across conditions as learning wore on, although rating error remained significantly greater in the configural compared to the elemental condition on the last (fifth) learning block (paired-sample T-test, behavioural sample $t_{32} = 4.69$, $p < 0.001$, Cohen's $d = 0.817$; fMRI sample $t_{41} = 6.46$, $p < 0.001$, Cohen's $d = 0.90$).

Along with the increase in accuracy, reaction times decreased across learning blocks (main effect of block, behavioural sample $F_{4, 288} = 7.17$ $p < 0.001$, $\eta^2_p = 0.09$; fMRI sample $F_{4, 369} = 26.38$, $p < 0.001$, $\eta^2_p = 0.22$). Reaction times were significantly faster in the elemental compared to the configural condition (main effect of condition, behavioural sample $F_{4, 288} = 467.58$, $p < 0.001$, $\eta^2_p = 0.62$; fMRI sample $F_{4, 369} = 391.35$, $p < 0.001$, $\eta^2_p = 0.51$). We found no significant block by condition interaction in the behavioural sample ($F_{4, 288} = 0.387$, $p = 0.818$, $\eta^2_p = 0.005$), but we did find a significant interaction in the fMRI sample ($F_{4, 369} = 4.35$, $p = 0.002$, $\eta^2_p = 0.05$).

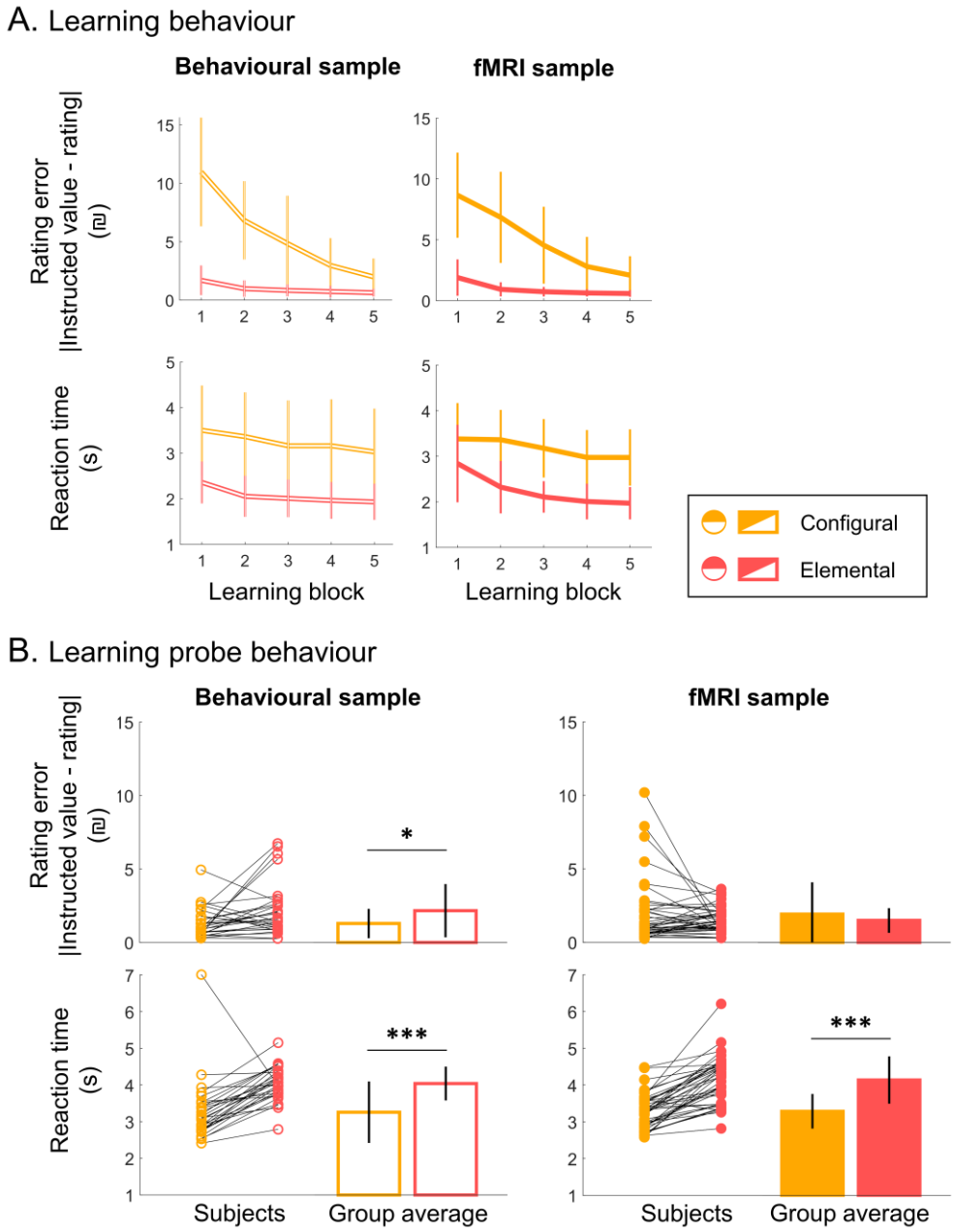

Figure 3. Accuracy and reaction time during the learning phase. A) Accuracy (top) and reaction time (bottom) across learning blocks in configural and elemental conditions. **B)** Accuracy (top) and reaction time (bottom) during the learning probe, by condition. Error bars represent one standard deviation. * Indicates a significant difference between conditions at $p < 0.05$, *** $p < 0.001$.

Learning probe

After five learning blocks, participants completed a learning probe without feedback, to assess the ability to assign value to the objects (**Fig. 3*B***). The learning probe was the first phase in which

participants had to sum two attribute-values in the elemental condition. This phase was also performed outside the scanner.

In the learning probe, accuracy was lower in the elemental condition compared to the configural condition in the behavioural sample (paired-sample T-test; $t_{32} = 2.13$, $p = 0.041$, Cohen's $d = 0.372$) but was not significantly different between conditions in the fMRI sample ($t_{41} = 1.30$, $p = 0.201$, Cohen's $d = 0.201$). Participants were slower in the elemental compared to the configural condition in both samples (behavioural sample $t_{32} = 5.47$, $p < 0.001$, Cohen's $d = 0.953$; fMRI sample $t_{41} = 9.56$, $p < 0.001$, Cohen's $d = 1.48$).

Bidding task

After learning, participants were shown objects from the configural and elemental sets and were asked to bid. Participants in the fMRI study performed the learning and probe phases outside the scanner and then performed the bidding stage while scanned with fMRI.

Bidding accuracy was high and not significantly different between the configural (mean rating error = 2.26NIS, SD = 1.66) and elemental (M = 2.04NIS, SD = 1.66) conditions for the behavioural sample ($t_{32} = 1.08$, $p = 0.289$, Cohen's $d = 0.188$) (**Fig. 4**). In the fMRI sample, bids tended to be closer to the instructed value (smaller error) in the elemental (M = 2.18NIS, SD = 1.02) compared to the configural condition (M = 2.55NIS, SD = 1.63), although the difference did not reach significance and the effect was marginal ($t_{41} = 1.90$, $p = 0.065$, Cohen's $d = 0.293$). Nevertheless, we included a trial-by-trial accuracy measure in the fMRI GLM analysis to control for this potential confound. Rating reaction times were not significantly different between conditions (behavioural sample $t_{32} = 1.80$, $p = 0.081$, Cohen's $d = 0.314$; fMRI sample $t_{41} = 0.251$, $p = 0.803$, Cohen's $d = 0.038$).

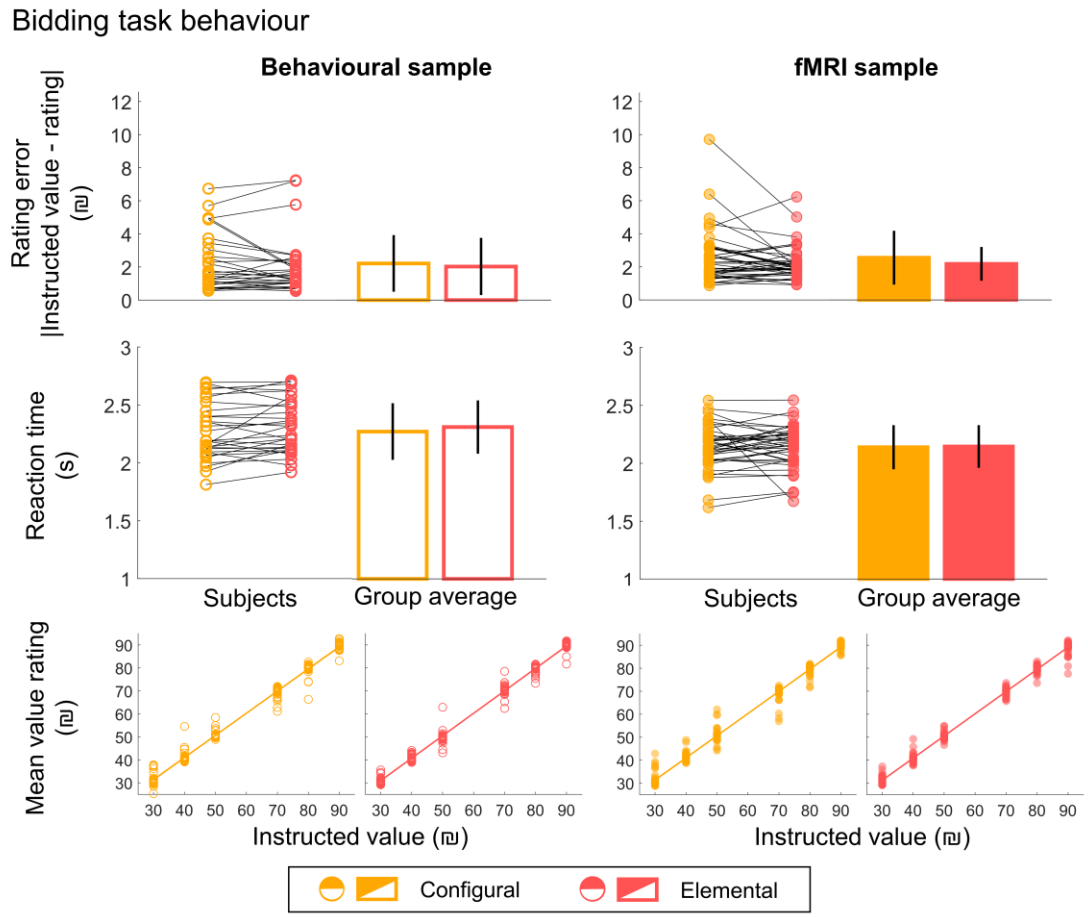

Figure 4. Accuracy and reaction time during the fMRI bidding phase. Individual and group average value rating error (top) and reaction time (middle) collapsed across all trials for each condition. Error bars represent one standard deviation from the group mean. Bottom panels show mean ratings for individual participants over the six presentations of each object with group-level linear regression fit.

Eye-tracking

We investigated whether eye movements during the 3-s object presentation epoch of the bidding task trials were different for objects learned in the elemental and configural condition (**Fig. 5**). The average number of fixations made on the whole object was similar between conditions (behavioural sample t_{32} = 1.741, p = 0.091, Cohen's d = 0.303; fMRI sample t_{32} = 0.479, p = 0.635, Cohen's d = 0.083). However, we found consistent condition differences across samples in eye movements with respect to fixations to the value-predictive attributes. Participants made significantly more transitions between these attributes in the configural compared to the elemental condition (behavioural sample t_{32} = 3.364, p = 0.002, Cohen's d = 0.586; fMRI sample t_{32} = 2.659, p = 0.012, Cohen's d = 0.463), and the average duration of individual

fixations was longer in the elemental condition (behavioural sample $t_{32} = 3.611$, $p = 0.001$, Cohen's $d = 0.559$; fMRI sample $t_{32} = 2.211$, $p = 0.034$, Cohen's $d = 0.385$).

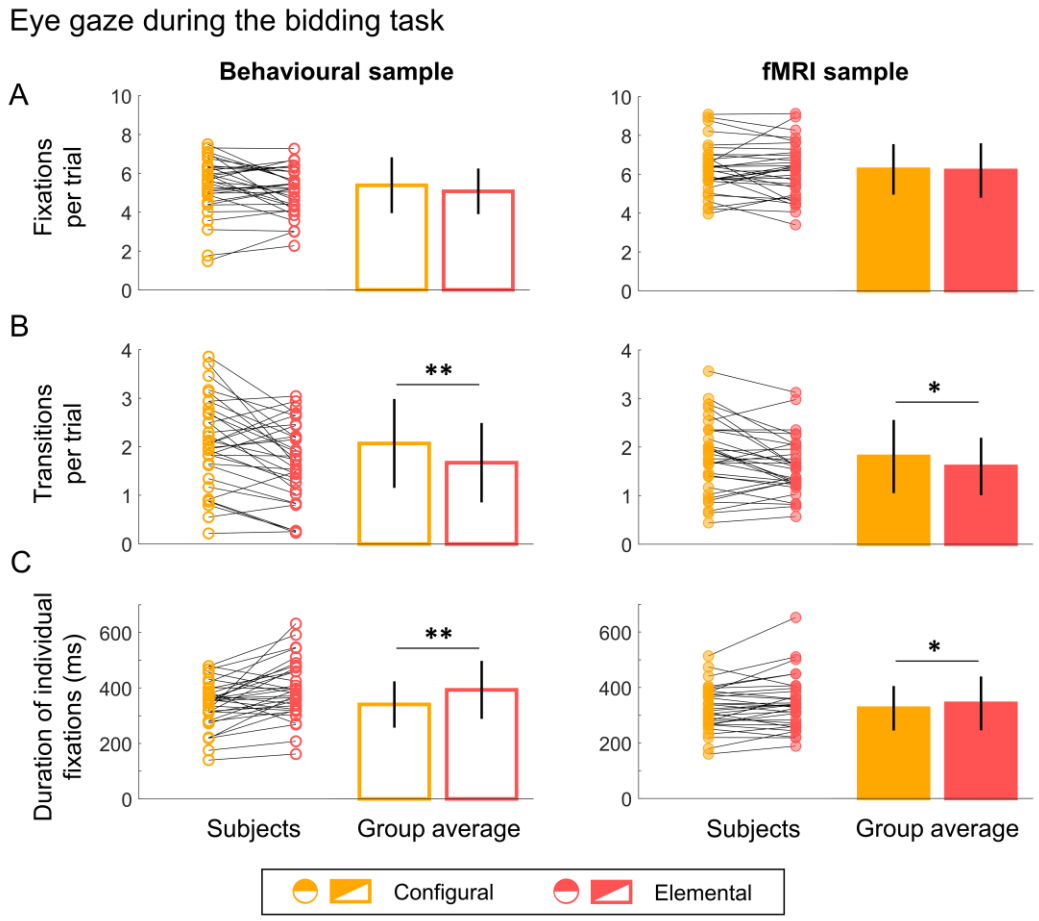

Figure 5. Eye-tracking results. Average number of fixations per trial (top), average number of transitions between attribute-AOIs per trial (middle) and average duration of individual fixations on attribute-AOIs (bottom). Error bars represent one standard deviation from the group mean. * indicate significant differences between conditions at $p < 0.05$, ** $p < 0.01$.

Brain imaging

vmPFC

We hypothesized that the fMRI signal in vmPFC would correlate with configural object value, and that the correlation of signal in vmPFC and value would be stronger for configural compared to elemental trials. To test this hypothesis, we preregistered analysis of value modulation effects at the time of object presentation in the *a priori* defined vmPFC region of interest using small volume correction. We did not

find the hypothesized value signal in the vmPFC during the object presentation epoch. Signal in this region did not significantly correlate with value in any condition and there was no significant condition by value interaction.

However, we found evidence in support of our hypothesis at the time of value rating. Two clusters in the vmPFC were significantly correlated with value for configural, but not elemental trials in the rating phase (**Fig. 6*A***). The direct condition contrast did not reveal a significant condition by value interaction, although this effect did emerge at a more liberal cluster-forming threshold of $Z = 2.3$, revealing a cluster in the vmPFC in which signal was correlated more strongly with value in configural compared to elemental trials, and in which signal correlated with value in configural trials (**Fig. 6*B***).

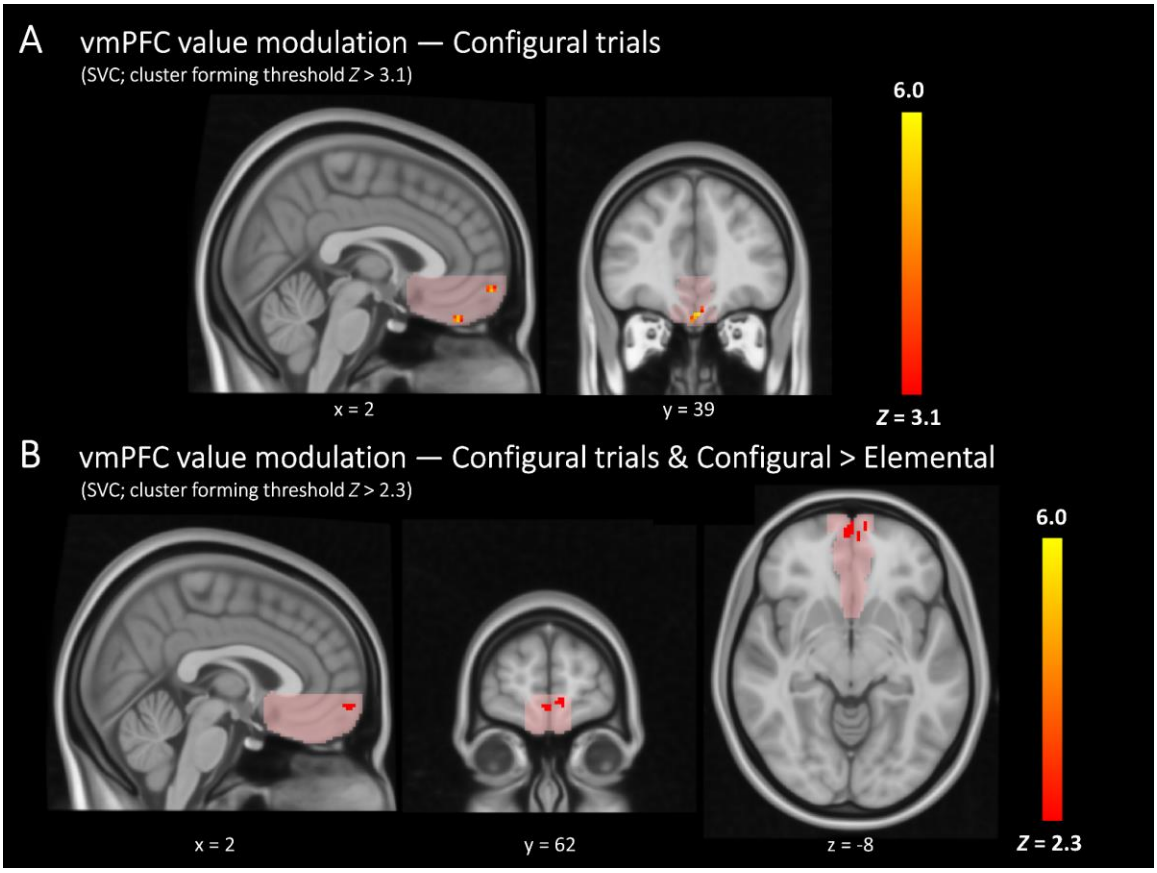

Figure 6. Value-modulated activation clusters during value rating in the vmPFC. A) Clusters where the fMRI signal was significantly modulated by value in Configural trials using the preregistered cluster forming threshold ($Z > 3.1$). **B)** Conjunction analysis using a more liberal cluster forming threshold of $Z > 2.3$ revealed a vmPFC cluster where signal was significantly modulated by value in Configural trials but not in Elemental trials, and where value modulation was stronger for Configural compared to Elemental trials. Results were small volume corrected (SVC)

for the pre-registered vmPFC region of interest (shaded area), $p < 0.05$. The color bar indicates Z-statistics. Numbers below slices indicate MNI coordinates. L = left, R = right.

Ventral visual stream

We next tested whether the ventral visual stream regions of interest were sensitive to valuation condition. Our preregistered hypothesis was that at the time of object presentation, signal in the PRC, and not in anterior VVS regions, would be greater when recognizing objects learned in the configural condition. We found no significant main effect of condition on BOLD in the PRC ($p = 0.460$) or any other VVS region (LOC $p = 0.286$; FFA $p = 0.731$; PPA $p = 0.136$) (**Fig. 7*B***, left) at the time of object presentation, indicating that during this time VVS ROIs were similarly activated in response to objects learned in the configural and elemental condition.

We next performed exploratory analyses to examine whether VVS regions were sensitive to value. We found a significant condition by value interaction in the PRC: in this region, the BOLD signal for subjective value was stronger for configural compared to elemental trials ($p = 0.016$, Bonferroni corrected for four ROIs) (**Fig. 7*B***, right). This effect was specific to the PRC and was not found in more posterior regions of the VVS (LOC, FFA and PPA uncorrected $ps > 0.727$). This effect was also specific to the object presentation epoch as there was no significant effect of condition (uncorrected $ps > 0.216$) and no condition by value interaction (uncorrected $ps > 0.394$) in any VVS regions during value ratings (**Fig. 7*C***). We note that signal in the PRC and other VVS regions did not demonstrate significant value modulation for the configural or elemental trials examined separately (Supplementary Material, **Fig. S2**).

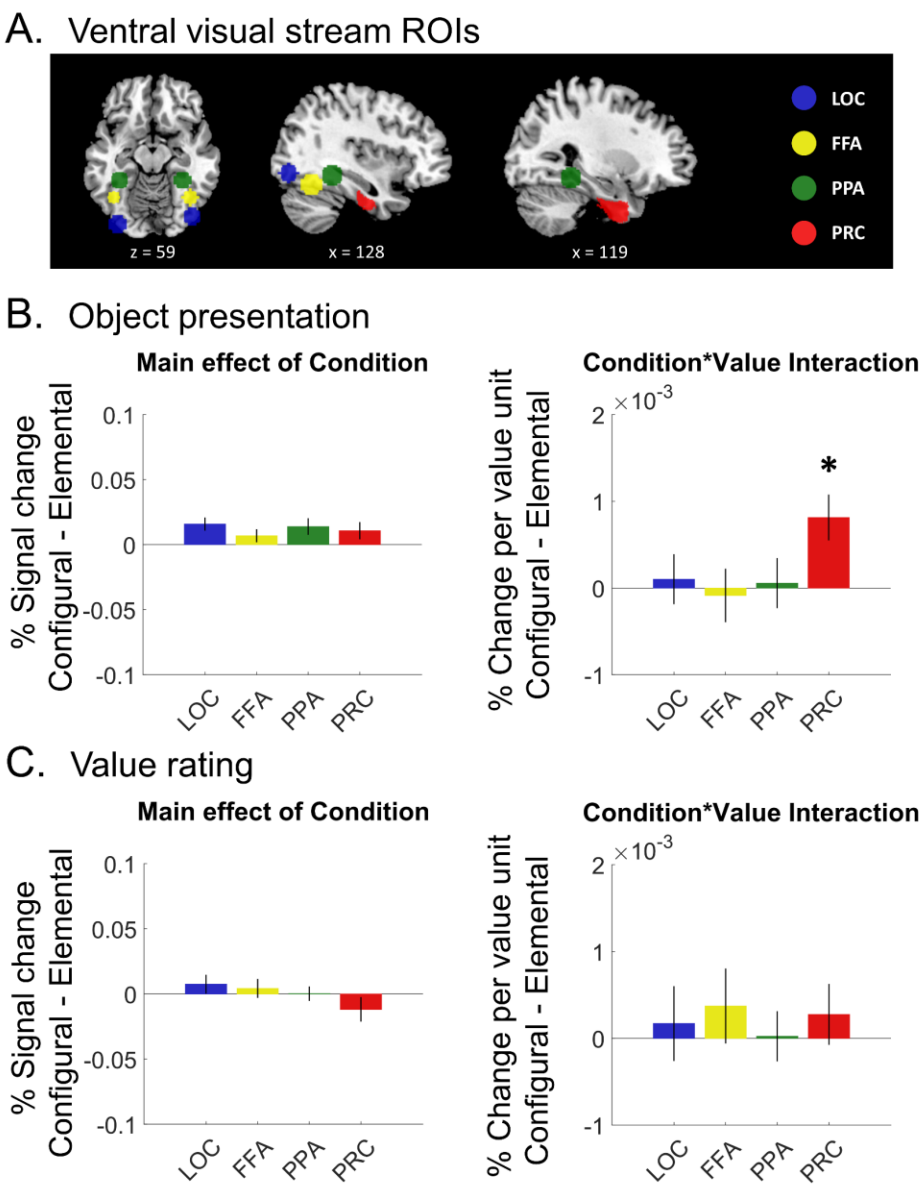

Figure 7. Ventral visual stream regions of interest analysis. A) Ventral visual stream regions of interest. The lateral occipital complex (LOC), fusiform face area (FFA) and parahippocampal place area (PPA) ROIs shown for a representative participant. The perirhinal cortex (PRC) ROI was the same for all participants. Numbers indicate coordinates in MNI space. **B)** Group average percent signal change during the object presentation epoch. **C)** Group average percent signal change at the value rating epoch. The left panels show the main effects of condition, assessed with the configural minus elemental trials contrast. The right panels show the condition by value interaction, assessed by contrasting the effect of value modulation in configural trials, minus value the effect of value modulation in elemental trials. Error bars represent SEM. Asterisk indicates significance at $p < 0.05$ for one sample t-test against 0, after Bonferroni correction for four comparisons.

Functional connectivity

We carried out exploratory (pre-registered) functional connectivity analysis using gPPI, defining the seed as the significant vmPFC clusters found for configural trials value modulation (**Fig. 6*A***). The gPPI analysis did not reveal any clusters across the whole-brain, and no VVS region displaying evidence for greater functional connectivity with the vmPFC seed in the configural compared to the elemental trials or vice versa.

Whole brain analyses

For completeness, we report exploratory whole brain analyses for the main effects of condition as well as the value modulation effects, during object presentation and value rating epochs. We accompany each figure with a table reporting the Pearson correlation between the group-level unthresholded statistical map and the 10 terms most strongly associated with this activation pattern across fMRI studies using the reverse inference tool of Neurosynth (Yarkoni et al. 2011). We first report the main effects of condition on brain activity at the time of object presentation.

Object presentation

The condition contrast revealed several brain regions that were significantly more active during the configural trials, including the right caudate, left lateral orbitofrontal cortex, the right inferior frontal gyrus, bilateral precuneus, bilateral lateral occipital complex and the cerebellum (**Fig. 8*A***). The opposite contrast revealed that primary sensory-motor cortex, supplementary motor cortex and the superior frontal gyrus were more active during elemental trials (**Fig. 8*B***). Complete information on all significant clusters is presented in Supplementary Material (**Table S1**). A cluster encompassing the left pre- and post-central gyrus correlated with object value in the two conditions (**Fig. 8*C-D***). This activation likely reflects motor preparation to report the value rating, as a longer index finger press was systematically associated with moving the slider to higher values on the scale.

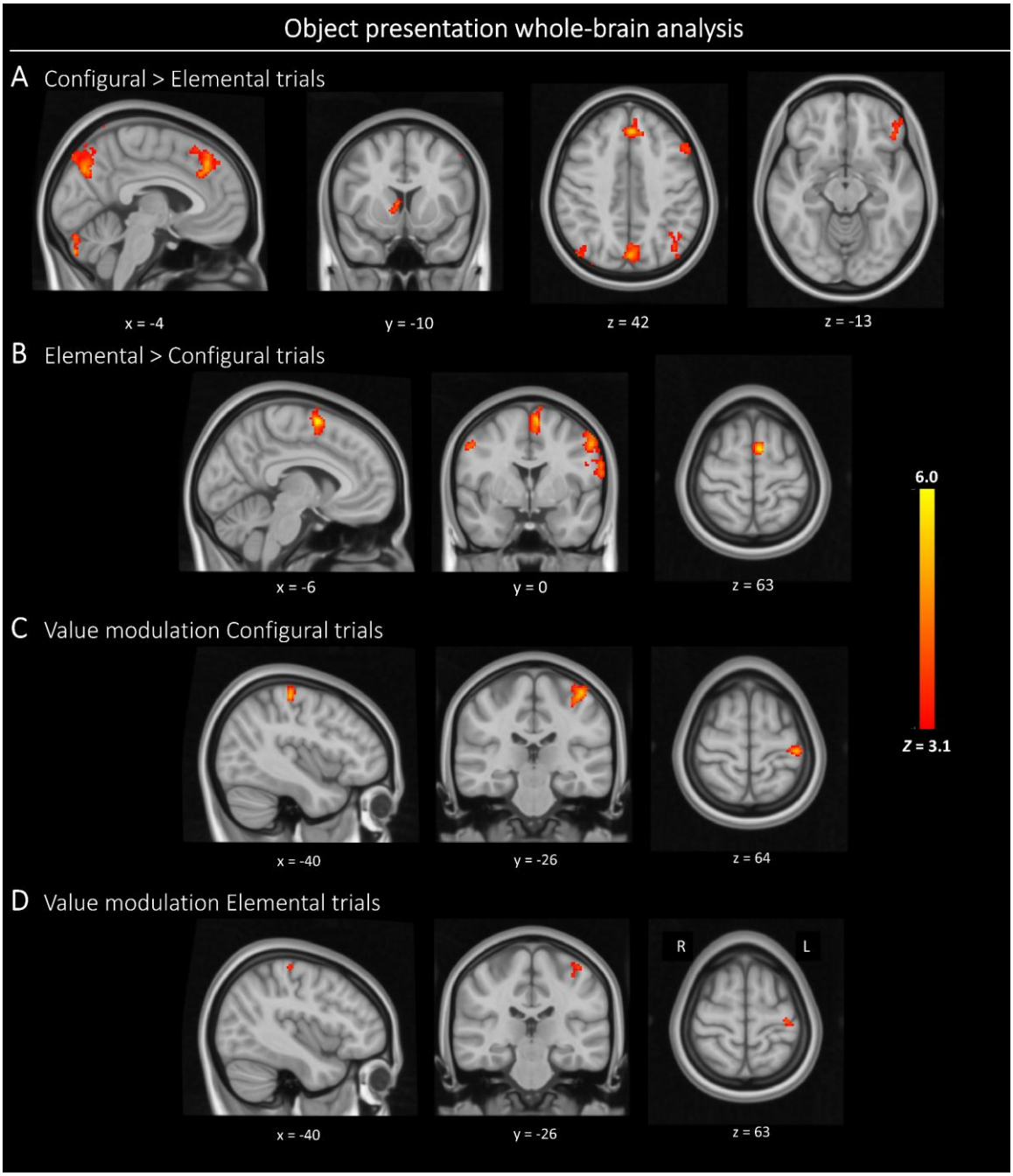

Figure 8. Whole-brain analysis of object presentation epoch. A) Clusters exhibiting greater activity in configural compared to elemental trials. **B)** Clusters exhibiting greater activity in elemental compared to configural trials. **C)** Clusters exhibiting value modulation in Configural trials. **D)** Clusters exhibiting value modulation in Elemental trials. Results were whole-brain cluster-corrected, $p < 0.05$. Color bar indicates Z-statistics. Numbers below slices indicate MNI coordinates. L = left, R = right.

Table 1. Pearson correlations between term-based reverse inference maps from Neurosynth and the unthresholded statistical maps of the contrasts shown in Fig. 8.

OBJECT PRESENTATION CONTRASTS	TERM	CORRELATION (R)
A) CONFIGURAL > ELEMENTAL	Retrieval	0.187
	Precuneus	0.176
	Episodic	0.145
	Memory retrieval	0.137
	Memory	0.122
	Recognition memory	0.122
	Episodic memory	0.114
	Semantic	0.111
	Navigation	0.101
	Retrosplenial	0.098
B) ELEMENTAL > CONFIGURAL	Motor	0.303
	Premotor	0.279
	Premotor cortex	0.262
	Movements	0.245
	Sensorimotor	0.238
	Motor imagery	0.237
	Supplementary	0.232
	Supplementary motor	0.225
	Primary motor	0.219
	Movement	0.218
C) VALUE MODULATION CONFIGURAL	Medial prefrontal	0.215
	Medial	0.19
	Social	0.155
	Resting	0.152
	Ventromedial	0.15
	Amygdala	0.147
	Resting state	0.146
	Orbitofrontal	0.143
	Emotional	0.142

	Mpfc	0.137
D) VALUE MODULATION ELEMENTAL	Fa	0.082
	Orbitofrontal	0.064
	Orbitofrontal cortex	0.063
	prefrontal	0.061
	Corpus	0.061
	Retrieval	0.061
	Corpus callosum	0.059
	Medial prefrontal	0.059
	Callosum	0.059
	Prefrontal cortex	0.058

Value rating

We did not find any clusters where activity was significantly greater in one condition compared to the other during the value rating epoch. Clusters common to both conditions contained signal, which was significantly modulated by value, including a cluster encompassing the pre- and post-central gyrus, in addition to occipital and fusiform clusters (**Fig. 9**). The fMRI signal did not correlate with value more in one condition compared to the other in any brain region.

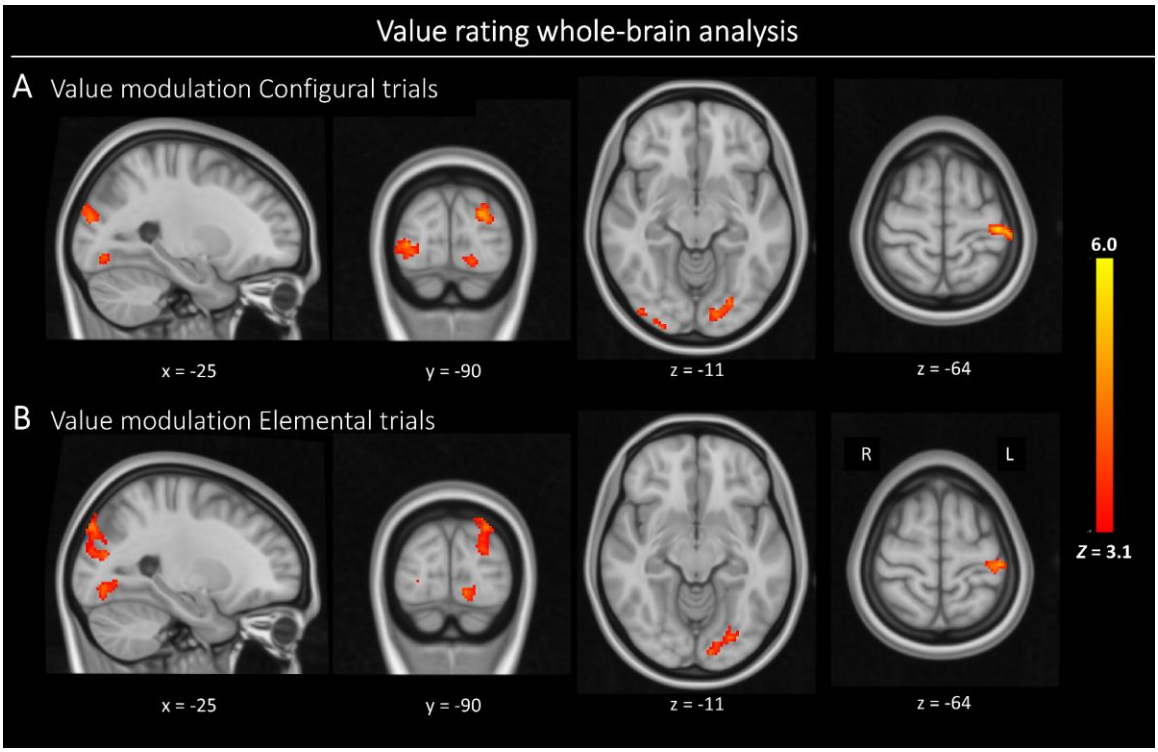

Figure 9. Whole brain analysis of the value rating epoch. A) Clusters exhibiting value modulation in Configural trials. **B)** Clusters exhibiting value modulation in Elemental trials. Results were whole-brain cluster-corrected, $p < 0.05$. Color bar indicates Z-statistics. Numbers below slices indicate MNI coordinates. L = left, R = right.

Table 2. Pearson correlations between term-based reverse inference maps from Neurosynth and the unthresholded statistical maps of the contrasts shown in Fig. 9.

VALUE RATING CONTRASTS	TERM	CORRELATION (R)
A) VALUE MODULATION CONFIGURAL	Medial prefrontal	0.187
	Medial	0.165
	Ventromedial	0.145
	Orbitofrontal	0.143
	Default	0.14
	Ventromedial prefrontal	0.136
	Autobiographical	0.136
	Orbitofrontal cortex	0.135
	Default mode	0.134
	Posterior cingulate	0.131

B) VALUE MODULATION ELEMENTAL	Hand movements	0.065
	Visual cortex	0.062
	Occipital	0.061
	Pitch	0.060
	Musical	0.059
	Planum temporale	0.059
	Auditory cortex	0.059
	Primary auditory	0.058
	Auditory	0.056
	Extrastriate	0.056

DISCUSSION

This study provides behavioural, eye-tracking and fMRI evidence that there are two ways to "see" the value of multi-attribute decision options. We found that evaluation of complex objects relied on different patterns of information acquisition, indexed by eye movements, and engaged different brain regions when value was predicted by configural relationships between attributes compared to when value could be added up from the values of individual attributes. Activity in the perirhinal cortex was related to value in configural more than elemental trials during object presentation, whereas at the time of value rating, the vmPFC showed value-modulated signal for configural trials only. Participants made more gaze transitions from one attribute to another when observing objects in the configural condition and made longer fixations on individual attributes in the elemental condition.

This study includes a replication of the behavioural and eye-tracking effects in two samples and inclusion of a pilot imaging sample to inform the design of the full fMRI experiment, which was pre-registered. Further, these experiments directly build on a recent study in patients with vmPFC damage using the same stimuli (Pelletier and Fellows 2019), providing converging evidence in keeping with the goal of triangulation (Munafò and Smith 2018). The lesion study found that vmPFC damage impaired binary decisions between fribbles in the configural condition, but not in the elemental condition (Pelletier and Fellows 2019). The current work provides additional support for the hypothesis that vmPFC has a unique role in inferring the value of objects based on configural information: BOLD signal in that region was only detectably modulated by object value in the configural and not the elemental condition. It further argues that evaluation under this condition engages the perirhinal cortex, a region known to be critical

for multi-attribute object recognition, but here for the first time also implicated in the evaluation of such objects.

We did not find that the total value of an object obtained by combining two separately learned attribute-values was reflected in the fMRI vmPFC signal. This null result alone cannot rule out that vmPFC is involved in value integration from multiple elements, but taken together with the finding that damage to vmPFC did not impair the ability to make choices based on such values, it suggests alternate mechanisms for value construction under such conditions, not requiring vmPFC.

Across a large body of existing fMRI work, vmPFC is reliably associated with subjective value (Bartra, McGuire, and Kable 2013; Rushworth and Behrens 2008). Activity in the vmPFC has previously been shown to reflect the value of items composed of multiple attributes, each modelled as independently predictive of value (Basten et al. 2010; Lim et al. 2013; Suzuki et al. 2017). One study using a very similar approach to the elemental condition here found that integrated value could be decoded from vmPFC signal using multivariate pattern analysis (MVPA) (Kahnt et al. 2011). MVPA has greater sensitivity to detect value-related signals that vary across participants and voxels than univariate analysis (Davis et al. 2014; Kahnt 2018). It is possible that we did not detect value related fMRI signals in the elemental condition in vmPFC using univariate analysis simply because this variable is represented more heterogeneously than in the configural condition. However, whereas a difference in coding scheme between conditions could partly explain our fMRI results, it is not consistent with the previous finding that vmPFC damage disrupts decisions in the configural but not the elemental condition.

Other neuroimaging studies of multi-attribute decision-making found correlates of value summed across attributes in other brain regions, not vmPFC (Berker et al. 2019; Fujiwara et al. 2009). The current findings add to the view that the vmPFC is not critical for value integration in general, but rather is engaged under a narrower set of conditions. We propose a more specific account whereby the vmPFC is required for inferring value from the configural relationships among lower-level attributes. This view might explain prior observations that patients with vmPFC damage are able to evaluate complex social or aesthetic stimuli, but seem to draw on different information to assess the value of such stimuli, compared to healthy participants (Vaidya, Sefranek, and Fellows 2018; Xia et al. 2015).

This current work also addressed whether regions known to be involved in complex object recognition are likewise involved in assessing the value of such options. Given previous findings of PRC activation in tasks requiring holistic object representation, but not in tasks accomplished on the basis of individual

attributes (Devlin and Price, 2007), and lesion studies demonstrating a causal role for PRC in configural object discrimination (Barense, Gaffan, and Graham 2007; Buckley and Gaffan 1998; Bussey, Saksida, and Murray 2002, 2003), we predicted greater activity in the PRC for evaluating objects in the configural condition. This hypothesis was not supported by our data, with no main effect of condition in the PRC or other VVS regions. It is possible that objects were processed similarly through the VVS in both conditions to support holistic recognition, as their general appearance (the body and position of appendages) was informative of whether a given stimulus was from the elemental or configural set. In any case, such holistic processing may be obligatory, even if not task-relevant.

However, we found that fMRI VVS signals were differently sensitive to value between conditions. Specifically, BOLD activity in the PRC was modulated by value more for configural compared to elemental trials. There are previous reports of value-correlated signal across the VVS, including in the primary visual cortex (Nelissen et al. 2012; Serences 2008), lateral occipital complex (Persichetti, Aguirre, and Thompson-Schill 2015), the PRC (Mogami and Tanaka 2006) and several of these regions combined (Arsenault et al. 2013; Kaskan et al. 2017). Across studies, reward has been paired with stimuli ranging in complexity from simple colored gratings to complex real-world objects, but no work previously contrasted conditions in which valuation relied on characteristics represented at different stages of the VVS hierarchy. Our findings suggest selective involvement of the PRC in encoding value when it is associated with the high-level (i.e. configural) object representation that this region supports.

The condition by value interaction observed for PRC activity was only observed at the time of object presentation, on average six seconds before the rating phase where value signal was detected in the vmPFC, arguing against the possibility that value-related PRC activation is driven by the vmPFC. The findings rather suggest that configural value emerges at least in part from activity in the VVS regions involved in holistic object recognition, with vmPFC activation following later. Electrophysiological recordings in macaques have found that PRC neurons are sensitive to object value slightly later than neurons of the immediately preceding VVS stage (area IT) (Mogami and Tanaka 2006), suggesting that value emerges along the VVS object processing stream. Mogami and Tanaka (2006) found that PRC neurons demonstrated value sensitivity at ~200 ms after stimulus onset, whereas other work reported value selectivity only after ~400-500ms in the OFC (Kennerley et al. 2008; Wallis and Miller 2003). Electroencephalography recordings in humans found that upon presentation of a reward-paired object, a value-correlated signal was detected rapidly in occipital cortex and traveled anteriorly to the prefrontal cortex as time passed (Larsen and O'Doherty 2014). With these data, the current work is

compatible with the recently proposed idea that value representations arise in a more distributed way, as information moves from sensory inputs to action generation (Yoo and Hayden 2018).

We did not find evidence for increased functional connectivity between the vmPFC and PRC (or any other brain region) during configural object valuation. This null result must be taken with caution, as the study was not powered to find such an effect. There are anatomical connections (Heide et al. 2013) and there is evidence of functional connectivity (Andrews-Hanna, Smallwood, and Spreng 2014) between the vmPFC and the medial temporal lobe in humans, and the PRC and medial OFC are reciprocally connected in macaques (Kondo, Saleem, and Price 2005). The current findings of value-related activations at different stages of the trial in the PRC and the vmPFC suggest that interactions between these two regions might be important for value estimation in configural conditions. Further work using methods with better temporal resolution will be needed to test this hypothesis.

We also found systematic differences in eye gaze patterns between conditions, replicated in two samples, one behavioural and one inside the MRI scanner. Fixations were shorter and more transitions were made between attributes of objects in the configural condition. Sequential sampling models have shown that value and gaze interact in driving the decision process (Krajbich, Armel, and Rangel 2010), and that gaze duration has a causal influence on value (Shimojo et al. 2003). However, little is known about fixation patterns within multi-attribute objects during choice (Krajbich 2019), and how they relate to the value construction process, regardless of expected value. Consumer research has extensively studied value construction strategies employed during multi-attribute decisions using process tracing measures including eye-tracking (Bettman, Luce, and Payne 1998; Russo and Dosher 1983). However, this work artificially decomposes options by laying out attributes as text and numbers in a matrix or table format, thus may not relate to everyday choices between real objects. Elucidating the interplay between gaze patterns and value construction for multi-attribute decisions where value predictions are based on visual information will be an important avenue of future research (Schonberg and Katz 2020).

Although we attempted to match the two conditions for difficulty, and further addressed this potential confound by controlling for trial-by-trial rating reaction time and accuracy in all fMRI analyses, we could not account for potential condition differences in speed of evaluation during the fixed object presentation time and the subsequent ITI. If evaluation is faster in the elemental condition, value-correlated signal might be passed on to motor regions earlier than in the configural condition (Hare et al. 2011; Yoo and Hayden 2018). The slider response requirement also meant that motor responses

were confounded with rated values, potentially explaining why motor regions showed value-correlated activation at the time of object presentation in the elemental condition.

In conclusion, this neuroimaging study, building directly on recent work in lesion patients provides evidence for two ways of building the value of complex objects, supported by at least partly distinct neural mechanisms. Leveraging object-recognition research to inform studies of multi-attribute value-based decisions, this work suggests that the relationship between attributes and value might influence how an object is processed through the VVS. Research at the interface of these two fields of study may bring fresh perspectives on the brain basis of both perception and motivated behavior.

REFERENCES

Andrews-Hanna, Jessica R., Jonathan Smallwood, and R. Nathan Spreng. 2014. "The Default Network and Self-Generated Thought: Component Processes, Dynamic Control, and Clinical Relevance." *Annals of the New York Academy of Sciences* 1316:29–52. doi: 10.1111/nyas.12360.

Arsenault, John T., Koen Nelissen, Bechir Jarraya, and Wim Vanduffel. 2013. "Dopaminergic Reward Signals Selectively Decrease FMRI Activity in Primate Visual Cortex." *Neuron* 77(6):1174–86. doi: 10.1016/j.neuron.2013.01.008.

Avants, B. B., C. L. Epstein, M. Grossman, and J. C. Gee. 2008. "Symmetric Diffeomorphic Image Registration with Cross-Correlation: Evaluating Automated Labeling of Elderly and Neurodegenerative Brain." *Medical Image Analysis* 12(1):26–41. doi: 10.1016/j.media.2007.06.004.

Barense, Morgan D., David Gaffan, and Kim S. Graham. 2007. "The Human Medial Temporal Lobe Processes Online Representations of Complex Objects." *Neuropsychologia* 45(13):2963–74. doi: 10.1016/j.neuropsychologia.2007.05.023.

Bartko, Susan J., Boyer D. Winters, Rosemary A. Cowell, Lisa M. Saksida, and Timothy J. Bussey. 2007. "Perirhinal Cortex Resolves Feature Ambiguity in Configural Object Recognition and Perceptual Oddity Tasks." *Learning & Memory (Cold Spring Harbor, N.Y.)* 14(12):821–32. doi: 10.1101/lm.749207.

Bartra, Oscar, Joseph T. McGuire, and Joseph W. Kable. 2013. "The Valuation System: A Coordinate-Based Meta-Analysis of BOLD FMRI Experiments Examining Neural Correlates of Subjective Value." *NeuroImage* 76:412–27. doi: 10.1016/j.neuroimage.2013.02.063.

Basten, Ulrike, Guido Biele, Hauke R. Heekeren, and Christian J. Fiebach. 2010. "How the Brain Integrates Costs and Benefits during Decision Making." *Proceedings of the National Academy of Sciences of the United States of America* 107(50):21767–72. doi: 10.1073/pnas.0908104107.

Behzadi, Yashar, Khaled Restom, Joy Liau, and Thomas T. Liu. 2007. "A Component Based Noise Correction Method (CompCor) for BOLD and Perfusion Based FMRI." *NeuroImage* 37(1):90–101. doi: 10.1016/j.neuroimage.2007.04.042.

Berker, Archy O. de, Zeb Kurth-Nelson, Robb B. Rutledge, Sven Bestmann, and Raymond J. Dolan. 2019. "Computing Value from Quality and Quantity in Human Decision-Making." *Journal of Neuroscience* 39(1):163–76. doi: 10.1523/JNEUROSCI.0706-18.2018.

Bettman, James R., Mary Frances Luce, and John W. Payne. 1998. "Constructive Consumer Choice Processes." *Journal of Consumer Research* 25(3):187–217. doi: 10.1086/209535.

Bombari, Dario, Fred W. Mast, and Janek S. Lobmaier. 2009. "Featural, Configural, and Holistic Face-Processing Strategies Evoke Different Scan Patterns." *Perception* 38(10):1508–21. doi: 10.1068/p6117.

Botvinik-Nezer, Rotem, Tom Salomon, and Tom Schonberg. 2020. "Enhanced Bottom-Up and Reduced Top-Down FMRI Activity Is Related to Long-Lasting Nonreinforced Behavioral Change." *Cerebral Cortex* 30(3):858–74. doi: 10.1093/cercor/bhz132.

Brainard, D. H. 1997. "The Psychophysics Toolbox." *Spatial Vision* 10(4):433–36.

Buckley, M. J., and D. Gaffan. 1998. "Perirhinal Cortex Ablation Impairs Configural Learning and Paired-Associate Learning Equally." *Neuropsychologia* 36(6):535–46.

Bussey, Timothy J., and Lisa M. Saksida. 2002. "The Organization of Visual Object Representations: A Connectionist Model of Effects of Lesions in Perirhinal Cortex." *The European Journal of Neuroscience* 15(2):355–64.

Bussey, Timothy J., Lisa M. Saksida, and Elisabeth A. Murray. 2002. "Perirhinal Cortex Resolves Feature Ambiguity in Complex Visual Discriminations." *The European Journal of Neuroscience* 15(2):365–74.

Bussey, Timothy J., Lisa M. Saksida, and Elisabeth A. Murray. 2003. "Impairments in Visual Discrimination after Perirhinal Cortex Lesions: Testing 'Declarative' vs. 'Perceptual-Mnemonic' Views of Perirhinal Cortex Function." *European Journal of Neuroscience* 17(3):649–60. doi: 10.1046/j.1460-9568.2003.02475.x.

Bussey, Timothy J., Lisa M. Saksida, and Elisabeth A. Murray. 2005. "The Perceptual-Mnemonic/Feature Conjunction Model of Perirhinal Cortex Function." *The Quarterly Journal of Experimental Psychology. B, Comparative and Physiological Psychology* 58(3–4):269–82. doi: 10.1080/02724990544000004.

Cox, Robert W., and James S. Hyde. 1997. "Software Tools for Analysis and Visualization of FMRI Data." *NMR in Biomedicine* 10(4–5):171–78. doi: 10.1002/(SICI)1099-1492(199706/08)10:4/5<171::AID-NBM453>3.0.CO;2-L.

Dale, A. M., B. Fischl, and M. I. Sereno. 1999. "Cortical Surface-Based Analysis. I. Segmentation and Surface Reconstruction." *NeuroImage* 9(2):179–94. doi: 10.1006/nimg.1998.0395.

Davis, Tyler, Karen F. LaRocque, Jeanette Mumford, Kenneth A. Norman, Anthony D. Wagner, and Russell A. Poldrack. 2014. "What Do Differences Between Multi-Voxel and Univariate Analysis Mean? How Subject-, Voxel-, and Trial-Level Variance Impact FMRI Analysis." *NeuroImage* 97:271–83. doi: 10.1016/j.neuroimage.2014.04.037.

Deichmann, R., J. A. Gottfried, C. Hutton, and R. Turner. 2003. "Optimized EPI for FMRI Studies of the Orbitofrontal Cortex." *NeuroImage* 19(2 Pt 1):430–41.

Delgado, Mauricio R., Jennifer S. Beer, Lesley K. Fellows, Scott A. Huettel, Michael L. Platt, Gregory J. Quirk, and Daniela Schiller. 2016. "Viewpoints: Dialogues on the Functional Role of the Ventromedial Prefrontal Cortex." *Nature Neuroscience* 19:1545–52. doi: 10.1038/nn.4438.

Devlin, Joseph T., and Cathy J. Price. 2007. "Perirhinal Contributions to Human Visual Perception." *Current Biology: CB* 17(17):1484–88. doi: 10.1016/j.cub.2007.07.066.

Duncan, Katherine, Bradley B. Doll, Nathaniel D. Daw, and Daphna Shohamy. 2018. "More Than the Sum of Its Parts: A Role for the Hippocampus in Configural Reinforcement Learning." *Neuron* 98(3):645-657.e6. doi: 10.1016/j.neuron.2018.03.042.

Erez, Jonathan, Rhodri Cusack, William Kendall, and Morgan D. Barense. 2016. "Conjunctive Coding of Complex Object Features." *Cerebral Cortex* 26(5):2271–82. doi: 10.1093/cercor/bhv081.

Esteban, Oscar, Christopher J. Markiewicz, Ross W. Blair, Craig A. Moodie, A. Ilkay Isik, Asier Erramuzpe, James D. Kent, Mathias Goncalves, Elizabeth DuPre, Madeleine Snyder, Hiroyuki Oya, Satrajit S. Ghosh, Jessey Wright, Joke Durnez, Russell A. Poldrack, and Krzysztof J. Gorgolewski. 2019. "FMRIPrep: A Robust Preprocessing Pipeline for Functional MRI." *Nature Methods* 16(1):111. doi: 10.1038/s41592-018-0235-4.

Fonov, VS, AC Evans, RC McKinstry, CR Almli, and DL Collins. 2009. "Unbiased Nonlinear Average Age-Appropriate Brain Templates from Birth to Adulthood." *NeuroImage* 47:S102. doi: 10.1016/S1053-8119(09)70884-5.

Friston, K. J., S. Williams, R. Howard, R. S. Frackowiak, and R. Turner. 1996. "Movement-Related Effects in FMRI Time-Series." *Magnetic Resonance in Medicine* 35(3):346–55.

Fujiwara, Juri, Philippe N. Tobler, Masato Taira, Toshio Iijima, and Ken-Ichiro Tsutsui. 2009. "Segregated and Integrated Coding of Reward and Punishment in the Cingulate Cortex." *Journal of Neurophysiology* 101(6):3284–93. doi: 10.1152/jn.90909.2008.

Gitelman, Darren R., William D. Penny, John Ashburner, and Karl J. Friston. 2003. "Modeling Regional and Psychophysiologic Interactions in FMRI: The Importance of Hemodynamic Deconvolution." *NeuroImage* 19(1):200–207.

Gorgolewski, Krzysztof, Christopher D. Burns, Cindee Madison, Dav Clark, Yaroslav O. Halchenko, Michael L. Waskom, and Satrajit S. Ghosh. 2011. "Nipype: A Flexible, Lightweight and Extensible Neuroimaging Data Processing Framework in Python." *Frontiers in Neuroinformatics* 5:13. doi: 10.3389/fninf.2011.00013.

Gorgolewski, Krzysztof J., Tibor Auer, Vince D. Calhoun, R. Cameron Craddock, Samir Das, Eugene P. Duff, Guillaume Flandin, Satrajit S. Ghosh, Tristan Glatard, Yaroslav O. Halchenko, Daniel A. Handwerker, Michael Hanke, David Keator, Xiangrui Li, Zachary Michael, Camille Maumet, B. Nolan Nichols, Thomas E. Nichols, John Pellman, Jean-Baptiste Poline, Ariel Rokem, Gunnar Schaefer, Vanessa Sochat, William Triplett, Jessica A. Turner, Gaël Varoquaux, and Russell A. Poldrack. 2016. "The Brain Imaging Data Structure, a Format for Organizing and Describing Outputs of Neuroimaging Experiments." *Scientific Data* 3:160044. doi: 10.1038/sdata.2016.44.

Greve, Douglas N., and Bruce Fischl. 2009. "Accurate and Robust Brain Image Alignment Using Boundary-Based Registration." *NeuroImage* 48(1):63–72. doi: 10.1016/j.neuroimage.2009.06.060.

Hare, Todd A., Wolfram Schultz, Colin F. Camerer, John P. O'Doherty, and Antonio Rangel. 2011. "Transformation of Stimulus Value Signals into Motor Commands during Simple Choice." *Proceedings of the National Academy of Sciences* 108(44):18120–25. doi: 10.1073/pnas.1109322108.

Heide, Von Der, Rebecca J, Laura M. Skipper, Elizabeth Klobusicky, and Ingrid R. Olson. 2013. "Dissecting the Uncinate Fasciculus: Disorders, Controversies and a Hypothesis." *Brain* 136(6):1692–1707. doi: 10.1093/brain/awt094.

Hunt, Laurence T., Raymond J. Dolan, and Timothy E. J. Behrens. 2014. "Hierarchical Competitions Subserving Multi-Attribute Choice." *Nature Neuroscience* 17(11):1613–22. doi: 10.1038/nn.3836.

Jenkinson, Mark, Peter Bannister, Michael Brady, and Stephen Smith. 2002. "Improved Optimization for the Robust and Accurate Linear Registration and Motion Correction of Brain Images." *NeuroImage* 17(2):825–41. doi: 10.1006/nimg.2002.1132.

Kahnt, Thorsten. 2018. "A Decade of Decoding Reward-Related FMRI Signals and Where We Go from Here." *NeuroImage* 180(Pt A):324–33. doi: 10.1016/j.neuroimage.2017.03.067.

Kahnt, Thorsten, Jakob Heinzle, Soyoung Q. Park, and John-Dylan Haynes. 2011. "Decoding Different Roles for VmPFC and DlPFC in Multi-Attribute Decision Making." *NeuroImage* 56(2):709–15. doi: 10.1016/j.neuroimage.2010.05.058.

Kaskan, Peter M., Vincent D. Costa, Hana P. Eaton, Julie A. Zemskova, Andrew R. Mitz, David A. Leopold, Leslie G. Ungerleider, and Elisabeth A. Murray. 2017. "Learned Value Shapes Responses to Objects in Frontal and Ventral Stream Networks in Macaque Monkeys." *Cerebral Cortex* 27(5):2739–57. doi: 10.1093/cercor/bhw113.

Kennerley, Steven W., Aspandiar F. Dahmubed, Antonio H. Lara, and Jonathan D. Wallis. 2008. "Neurons in the Frontal Lobe Encode the Value of Multiple Decision Variables." *Journal of Cognitive Neuroscience* 21(6):1162–78. doi: 10.1162/jocn.2009.21100.

Klein, Arno, Satrajit S. Ghosh, Forrest S. Bao, Joachim Giard, Yrjö Häme, Eliezer Stavsky, Noah Lee, Brian Rossa, Martin Reuter, Elias Chaibub Neto, and Anisha Keshavan. 2017. "Mindboggling Morphometry of Human Brains." *PLOS Computational Biology* 13(2):e1005350. doi: 10.1371/journal.pcbi.1005350.

Kondo, Hideki, Kadharbatcha S. Saleem, and Joseph L. Price. 2005. "Differential Connections of the Perirhinal and Parahippocampal Cortex with the Orbital and Medial Prefrontal Networks in Macaque Monkeys." *The Journal of Comparative Neurology* 493(4):479–509. doi: 10.1002/cne.20796.

Krajbich, Ian. 2019. "Accounting for Attention in Sequential Sampling Models of Decision Making." *Current Opinion in Psychology* 29:6–11. doi: 10.1016/j.copsyc.2018.10.008.

Krajbich, Ian, Carrie Armel, and Antonio Rangel. 2010. "Visual Fixations and the Computation and Comparison of Value in Simple Choice." *Nature Neuroscience* 13(10):1292–98. doi: 10.1038/nn.2635.

Kurtz-David, Vered, Dotan Persitz, Ryan Webb, and Dino J. Levy. 2019. "The Neural Computation of Inconsistent Choice Behavior." *Nature Communications* 10(1):1583. doi: 10.1038/s41467-019-09343-2.

Lanczos, Cornelius. 1964. "Evaluation of Noisy Data." *Journal of the Society for Industrial and Applied Mathematics: Series B, Numerical Analysis* 1(1):76–85. doi: 10.1137/0701007.

Larsen, Tobias, and John P. O'Doherty. 2014. "Uncovering the Spatio-Temporal Dynamics of Value-Based Decision-Making in the Human Brain: A Combined FMRI–EEG Study." *Philosophical Transactions of the Royal Society B: Biological Sciences* 369(1655). doi: 10.1098/rstb.2013.0473.

Levy, Dino J., and Paul W. Glimcher. 2012. "The Root of All Value: A Neural Common Currency for Choice." *Current Opinion in Neurobiology* 22(6):1027–38. doi: 10.1016/j.conb.2012.06.001.

Lim, Seung-Lark, John P. O'Doherty, and Antonio Rangel. 2013. "Stimulus Value Signals in Ventromedial PFC Reflect the Integration of Attribute Value Signals Computed in Fusiform Gyrus and Posterior Superior Temporal Gyrus." *The Journal of Neuroscience* 33(20):8729–41. doi: 10.1523/JNEUROSCI.4809-12.2013.

McLaren, Donald G., Michele L. Ries, Guofan Xu, and Sterling C. Johnson. 2012. "A Generalized Form of Context-Dependent Psychophysiological Interactions (GPPI): A Comparison to Standard Approaches." *NeuroImage* 61(4):1277–86. doi: 10.1016/j.neuroimage.2012.03.068.

Mogami, Tsuguo, and Keiji Tanaka. 2006. "Reward Association Affects Neuronal Responses to Visual Stimuli in Macaque TE and Perirhinal Cortices." *Journal of Neuroscience* 26(25):6761–70. doi: 10.1523/JNEUROSCI.4924-05.2006.

Mumford, Jeanette A. 2007. *A Guide to Calculating Percent Change with Featquery*.

Mumford, Jeanette A., and Thomas Nichols. 2008. "Power Calculation for Group FMRI Studies Accounting for Arbitrary Design and Temporal Autocorrelation." *NeuroImage* 39(1):261–68. doi: 10.1016/j.neuroimage.2007.07.061.

Munafò, Marcus R., and George Davey Smith. 2018. "Robust Research Needs Many Lines of Evidence." *Nature* 553(7689):399–401. doi: 10.1038/d41586-018-01023-3.

Murray, Elisabeth A., Timothy J. Bussey, and Lisa M. Saksida. 2007. "Visual Perception and Memory: A New View of Medial Temporal Lobe Function in Primates and Rodents." *Annual Review of Neuroscience* 30(1):99–122. doi: 10.1146/annurev.neuro.29.051605.113046.

Nelissen, Koen, Béchir Jarraya, John T. Arsenault, Bruce R. Rosen, Lawrence L. Wald, Joseph B. Mandeville, John J. Marota, and Wim Vanduffel. 2012. "Neural Correlates of the Formation and Retention of Cocaine-Induced Stimulus-Reward Associations." *Biological Psychiatry* 72(5):422–28. doi: 10.1016/j.biopsych.2012.02.021.

Park, Soyoung Q., Thorsten Kahnt, Jörg Rieskamp, and Hauke R. Heekeren. 2011. "Neurobiology of Value Integration: When Value Impacts Valuation." *The Journal of Neuroscience: The Official Journal of the Society for Neuroscience* 31(25):9307–14. doi: 10.1523/JNEUROSCI.4973-10.2011.

Pelletier, Gabriel, and Lesley K. Fellows. 2019. "A Critical Role for Human Ventromedial Frontal Lobe in Value Comparison of Complex Objects Based on Attribute Configuration." *The Journal of Neuroscience* 39(21):4124–32. doi: 10.1523/JNEUROSCI.2969-18.2019.

Persichetti, Andrew S., Geoffrey K. Aguirre, and Sharon L. Thompson-Schill. 2015. "Value Is in the Eye of the Beholder: Early Visual Cortex Codes Monetary Value of Objects during a Diverted Attention Task." *Journal of Cognitive Neuroscience* 27(5):893–901. doi: 10.1162/jocn_a_00760.

Philiastides, Marios G., Guido Biele, and Hauke R. Heekeren. 2010. "A Mechanistic Account of Value Computation in the Human Brain." *Proceedings of the National Academy of Sciences of the United States of America* 107(20):9430–35. doi: 10.1073/pnas.1001732107.

Power, Jonathan D., Anish Mitra, Timothy O. Laumann, Abraham Z. Snyder, Bradley L. Schlaggar, and Steven E. Petersen. 2014. "Methods to Detect, Characterize, and Remove Motion Artifact in Resting State FMRI." *NeuroImage* 84:320–41. doi: 10.1016/j.neuroimage.2013.08.048.

Riesenhuber, M., and T. Poggio. 1999. "Hierarchical Models of Object Recognition in Cortex." *Nature Neuroscience* 2(11):1019–25. doi: 10.1038/14819.

Rushworth, Matthew F. S., and Timothy E. J. Behrens. 2008. "Choice, Uncertainty and Value in Prefrontal and Cingulate Cortex." *Nature Neuroscience* 11(4):389–97. doi: 10.1038/nn2066.

Russo, J. E., and B. A. Dosher. 1983. "Strategies for Multiattribute Binary Choice." *Journal of Experimental Psychology. Learning, Memory, and Cognition* 9(4):676–96. doi: 10.1037//0278-7393.9.4.676.

Salomon, Tom, Rotem Botvinik-Nezer, Shiran Oren, and Tom Schonberg. 2020. "Enhanced Striatal and Prefrontal Activity Is Associated with Individual Differences in Nonreinforced Preference Change for Faces." *Human Brain Mapping* 41(4):1043–60. doi: 10.1002/hbm.24859.

Schonberg, Tom, Akram Bakkour, Ashleigh M. Hover, Jeanette A. Mumford, Lakshya Nagar, Jacob Perez, and Russell A. Poldrack. 2014. "Changing Value through Cued Approach: An Automatic Mechanism of Behavior Change." *Nature Neuroscience* 17(4):625–30. doi: 10.1038/nn.3673.

Schonberg, Tom, and Leor N. Katz. 2020. "A Neural Pathway for Nonreinforced Preference Change." *Trends in Cognitive Sciences* 0(0). doi: 10.1016/j.tics.2020.04.002.

Serences, John T. 2008. "Value-Based Modulations in Human Visual Cortex." *Neuron* 60(6):1169–81. doi: 10.1016/j.neuron.2008.10.051.

Shimojo, Shinsuke, Claudiu Simion, Eiko Shimojo, and Christian Scheier. 2003. "Gaze Bias Both Reflects and Influences Preference." *Nature Neuroscience* 6(12):1317–22. doi: 10.1038/nn1150.

Smith, Stephen M., Mark Jenkinson, Mark W. Woolrich, Christian F. Beckmann, Timothy E. J. Behrens, Heidi Johansen-Berg, Peter R. Bannister, Marilena De Luca, Ivana Drobnjak, David E. Flitney, Rami K. Niazy, James Saunders, John Vickers, Yongyue Zhang, Nicola De Stefano, J. Michael Brady, and Paul M. Matthews. 2004. "Advances in Functional and Structural MR Image Analysis and Implementation as FSL." *NeuroImage* 23 Suppl 1:S208-219. doi: 10.1016/j.neuroimage.2004.07.051.

Suzuki, Shinsuke, Logan Cross, and John P. O'Doherty. 2017. "Elucidating the Underlying Components of Food Valuation in the Human Orbitofrontal Cortex." *Nature Neuroscience* 20(12):1780–86. doi: 10.1038/s41593-017-0008-x.

Tustison, N. J., B. B. Avants, P. A. Cook, Y. Zheng, A. Egan, P. A. Yushkevich, and J. C. Gee. 2010. "N4ITK: Improved N3 Bias Correction." *IEEE Transactions on Medical Imaging* 29(6):1310–20. doi: 10.1109/TMI.2010.2046908.

Vaidya, Avinash R., Marcus Sefranek, and Lesley K. Fellows. 2018. "Ventromedial Frontal Lobe Damage Alters How Specific Attributes Are Weighed in Subjective Valuation." *Cerebral Cortex* 28(11):3857–67. doi: 10.1093/cercor/bhx246.

Wallis, Jonathan D., and Earl K. Miller. 2003. "Neuronal Activity in Primate Dorsolateral and Orbital Prefrontal Cortex during Performance of a Reward Preference Task." *The European Journal of Neuroscience* 18(7):2069–81. doi: 10.1046/j.1460-9568.2003.02922.x.

Watson, Hilary C., Edward L. Wilding, and Kim S. Graham. 2012. "A Role for Perirhinal Cortex in Memory for Novel Object–Context Associations." *Journal of Neuroscience* 32(13):4473–81. doi: 10.1523/JNEUROSCI.5751-11.2012.

Williams, Pepper. 1998. "Representational Organization of Multiple Exemplars of Object Categories." *University of Massachusetts at Boston*.

Xia, Chenjie, Dietlind Stolle, Elisabeth Gidengil, and Lesley K. Fellows. 2015. "Lateral Orbitofrontal Cortex Links Social Impressions to Political Choices." *The Journal of Neuroscience* 35(22):8507–14. doi: 10.1523/JNEUROSCI.0526-15.2015.

Yarkoni, Tal, Russell A. Poldrack, Thomas E. Nichols, David C. Van Essen, and Tor D. Wager. 2011. "Large-Scale Automated Synthesis of Human Functional Neuroimaging Data." *Nature Methods* 8(8):665–70. doi: 10.1038/nmeth.1635.

Yoo, Seng Bum Michael, and Benjamin Yost Hayden. 2018. "Economic Choice as an Untangling of Options into Actions." *Neuron* 99(3):434–47. doi: 10.1016/j.neuron.2018.06.038.

Zhang, Y., M. Brady, and S. Smith. 2001. "Segmentation of Brain MR Images through a Hidden Markov Random Field Model and the Expectation-Maximization Algorithm." *IEEE Transactions on Medical Imaging* 20(1):45–57. doi: 10.1109/42.906424.

SUPPLEMENTARY MATERIAL

Table S1. Regions showing significant activations clusters for whole brain imaging contrasts presented in Fig. 7 and Fig. 8. For each cluster, the list shows all regions from the Harvard-Oxford atlas that contained more than 5 voxels within that cluster, along with the peak X/Y/Z location for the cluster in MNI space

Contrast	Cluster #	Cluster size	X	Y	Z	Peak Z-value	p	Region	# of voxels in region
Configural > Elemental Object Presentation	1	65	8	8	6	4.980	0.0168		
								R._Caudate	34
	2	77	40	-68	-46	4.900	0.00635		
								Cerebellum	77
	3	176	56	28	22	4.580	7.69e-06		
								R._Inferior_Frontal_Gyrus_pars_triangularis	44
								R._Middle_Frontal_Gyrus	35
								R._Inferior_Frontal_Gyrus_pars_opercularis	13
								R._Frontal_Pole	8
	4	184	-44	-60	46	4.110	4.77e-06		
								L._Lateral_Occipital_Cortex_superior_division	118
								L._Angular_Gyrus	32
	5	193	14	-68	28	4.340	2.8e-06		
								R._Precuneous_Cortex	183
	6	307	42	-74	48	4.760	6.25e-09		
								R._Lateral_Occipital_Cortex_superior_division	262
	7	354	-14	-82	-36	5.200	6.34e-10		
								Cerebellum	290
	8	374	-2	36	42	5.320	2.47e-10		
								L._Superior_Frontal_Gyrus	189
								L._Paracingulate_Gyrus	106
								R._Superior_Frontal_Gyrus	29
								R._Paracingulate_Gyrus	16
	9	478	14	-72	-30	5.720	2.35e-12		
								Cerebellum	370
	10	1060	-38	22	-4	4.940	9.6e-22		
								L._Frontal_Pole	358
								L._Middle_Frontal_Gyrus	148
								L._Frontal_Orbital_Cortex	116
								L._Inferior_Frontal_Gyrus_pars_triangularis	115

								L._Insular_Cortex	21
								L._Inferior_Frontal_Gyrus_pars_opercularis	12
	11	1097	2	-68	60	5.060	2.85e-22		
								L._Precuneous_Cortex	650
								R._Precuneous_Cortex	150
								L._Cuneal_Cortex	45
								R._Cuneal_Cortex	12

Contrast	Cluster #	Cluster size	X	Y	Z	Peak Z-value	p	Region	# of voxels in region
Elemental > Configural Object Presentation	1	67	54	-2	40	5.200	0.0142		
								R._Precentral_Gyrus	67
	2	219	-6	2	64	6.160	6.56e-07		
								L._Juxtapositional_Lobule_Cortex_(formerly _Supplementary_Motor_Cortex)	174
								L._Superior_Frontal_Gyrus	19
	3	288	-64	8	22	5.290	1.63e-08		
								L._Precentral_Gyrus	185
								L._Inferior_Frontal_Gyrus_pars_opercularis	19
	4	505	-56	-4	38	5.520	7.42e-13		
								L._Precentral_Gyrus	372
								L._Postcentral_Gyrus	16

Contrast	Cluster #	Cluster size	X	Y	Z	Peak Z-value	p	Region	# of voxels in region
Configural Object Presentation modulated by Value	1	172	-42	-26	62	5.340	3.34e-06		
								L._Postcentral_Gyrus	138
								L._Precentral_Gyrus	19

Contrast	Cluster #	Cluster size	X	Y	Z	Peak Z-value	p	Region	# of voxels in region
Elemental Object Presentation modulated by Value	1	56	-36	-22	64	4.150	0.0231		
								L._Postcentral_Gyrus	40
								L._Precentral_Gyrus	16

Contrast	Cluster #	Cluster size	X	Y	Z	Peak Z-value	p	Region	# of voxels in region
Elemental trials Rating Scale modulated by Value	1	110	-46	-78	6	4.930	0.000254		
								L._Lateral_Occipital_Cortex_inferior_division	66
								L._Lateral_Occipital_Cortex_superior_division	37

	2	147	-22	-88	22	5.090	1.78e-05		
								L._Lateral_Occipital_Cortex_superior_division	75
								L._Occipital_Pole	70
	3	165	-14	-86	-16	5.050	5.3e-06		
								L._Occipital_Fusiform_Gyrus	117
								L._Occipital_Pole	21
								L._Lingual_Gyrus	15
	4	273	-42	-26	62	6.060	7.83e-09		
								L._Postcentral_Gyrus	158
								L._Precentral_Gyrus	50
	5	367	26	-98	0	5.110	5.36e-11		
								R._Occipital_Pole	270
								R._Lateral_Occipital_Cortex_inferior_division	92

Contrast	Cluster #	Cluster size	X	Y	Z	Peak Z-value	p	Region	# of voxels in region
Elemental trials Rating Scale modulated by Value	1	117	28	-94	2	4.550	0.000178		
								R._Occipital_Pole	116
	2	205	-44	-26	62	5.120	5.36e-07	L._Postcentral_Gyrus	157
								L._Postcentral_Gyrus	157
								L._Precentral_Gyrus	32
	3	237	-48	-78	18	4.750	5.96e-08		
								L._Lateral_Occipital_Cortex_inferior_division	171
								L._Lateral_Occipital_Cortex_superior_division	38
	4	242	-16	-84	-10	4.620	5.96e-08		
								L._Occipital_Fusiform_Gyrus	166
								L._Occipital_Pole	23
								L._Lingual_Gyrus	16
	5	411	-24	-86	34	4.690	9.17e-12		
								L._Lateral_Occipital_Cortex_superior_division	281
								L._Occipital_Pole	59

Contrast	Cluster #	Cluster size	X	Y	Z	Peak Z-value	p	Region	# of voxels in region
Configural Rating Scale modulated by Value, SVC for vmPFC ROI	1	15	-4	30	-26	3.780	0.0376		
								L._Subcallosal_Cortex	8
								L._Frontal_Medial_Cortex	6
	2	17	2	60	-10	3.720	0.0283		
								R._Frontal_Pole	13

	3	18	0	40	-26	3.940	0.0247	
							L._Frontal_Medial_Cortex	12
							R._Frontal_Medial_Cortex	6

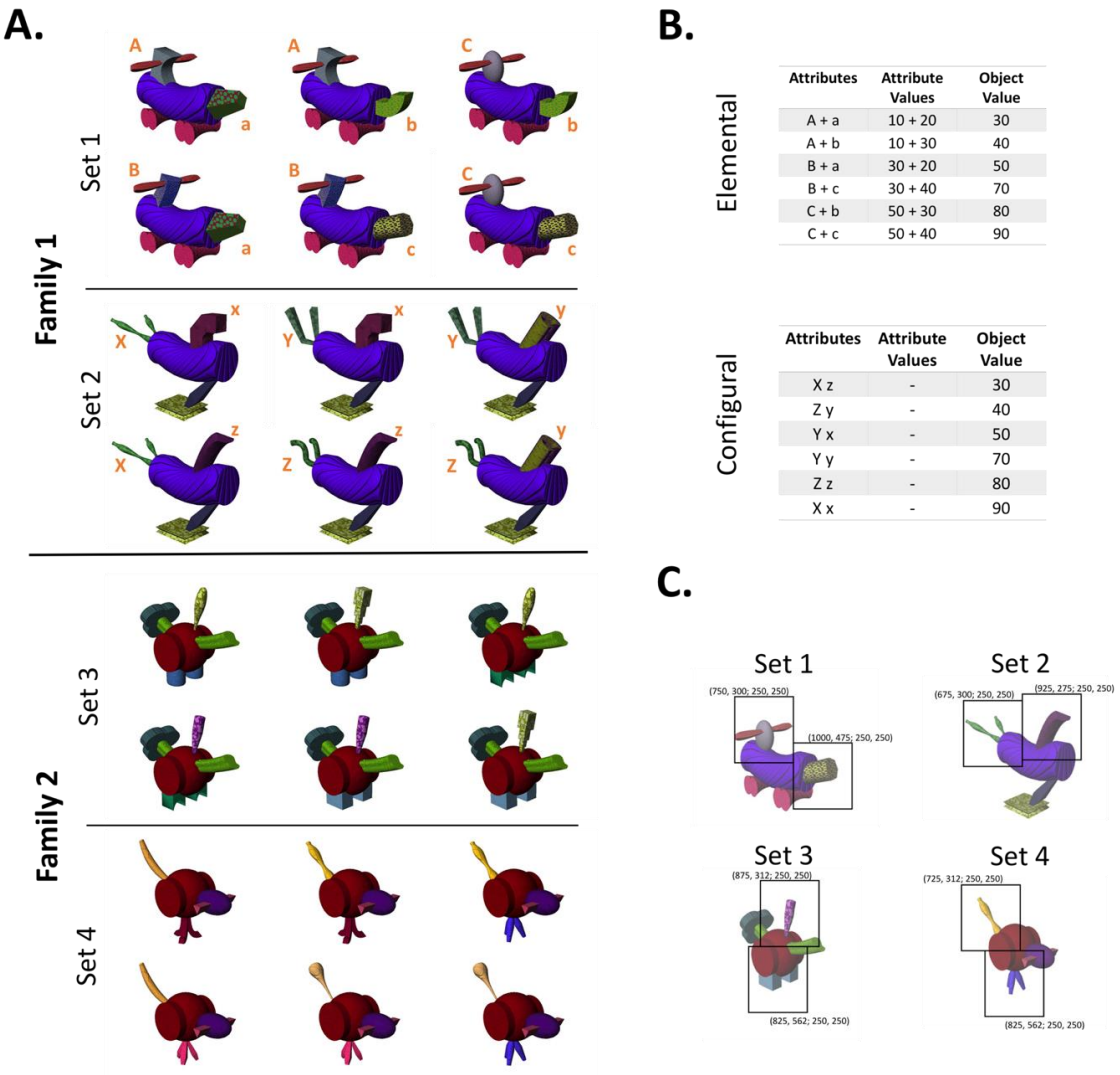

Figure S1. Object sets, object-value associations and areas of interest used for eye-tracking analysis. **A)** Object sets. Each participant is assigned one of the two fribbles families. Each condition is then assigned one object set from the selected family. The condition-object set pairing is counterbalanced across participants. **B)** Example of object value-association for one participant. **C)** Pre-registered areas of interest (AOI) for eye-tracking analysis, overlaid on an example object for each of the 4 object sets. AOIs are identical for all six objects within each object set. Numbers indicate (x origin, y origin; height; width) in screen pixels.

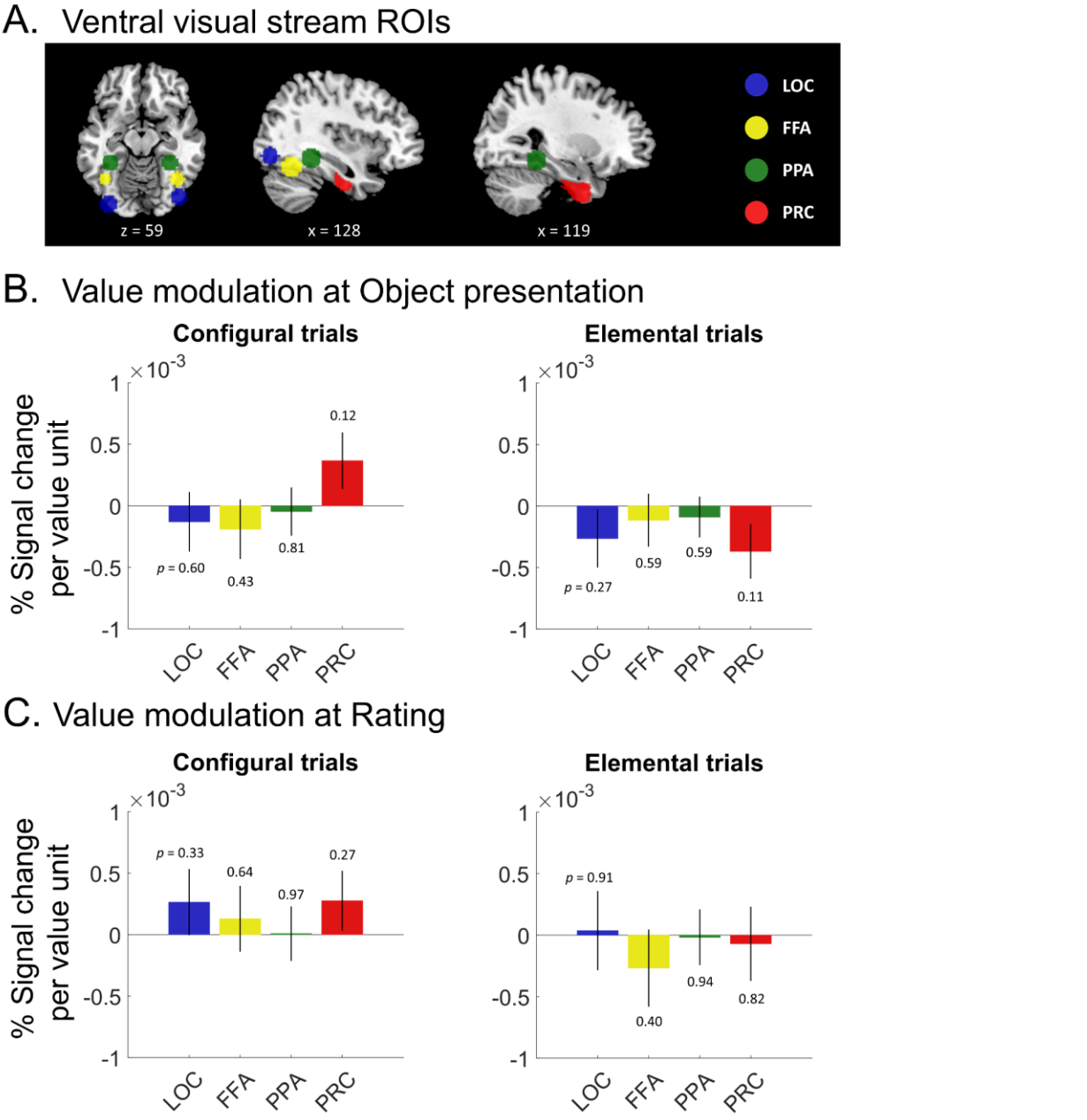

Figure S2. Value modulation in ventral visual stream regions of interest. A) Ventral visual stream regions of interest. The lateral occipital complex (LOC), fusiform face area (FFA) and parahippocampal place area (PPA) ROIs shown for a representative participant. The perirhinal cortex (PRC) ROI was the same for all participants. Numbers indicate coordinates in MNI space. **B)** Average contrasts of parameter estimate for value modulation at the object presentation epoch. **C)** Average contrasts of parameter estimate for value modulation at the rating epoch. Error bars represent SEM. Numbers above or bellow bars indicate uncorrected *p*-values for one-sample t-tests against 0 (baseline).